

1 Depleting cationic lipids involved in antimicrobial resistance drives  
2 adaptive lipid remodeling in *Enterococcus faecalis*

3 Rafi Rashid<sup>1,2#</sup>, Zeus Jaren Nair<sup>2,3,4#</sup>, Dominic Ming Hao Chia<sup>2,4</sup>, Kelvin Kian Long Chong<sup>2,4</sup>,  
4 Amaury Cazenave Gassiot<sup>5,6</sup>, Stewart A. Morley<sup>7,8</sup>, Doug K. Allen<sup>7,8</sup>, Swaine L. Chen<sup>8,9</sup>, Shu Sin  
5 Chng<sup>2,10</sup>, Markus R. Wenk<sup>5,6</sup>, Kimberly A. Kline<sup>2,4,11\*</sup>

6 <sup>1</sup>Integrative Sciences & Engineering Programme, National University of Singapore, Singapore

7 <sup>2</sup>Singapore Centre for Environmental Life Sciences Engineering, Nanyang Technological  
8 University, Singapore

9 <sup>3</sup>Interdisciplinary Graduate School, Nanyang Technological University, Singapore

10 <sup>4</sup>School of Biological Sciences, Nanyang Technological University, Singapore

11 <sup>5</sup>Singapore Lipidomics Incubator (SLING), Life Sciences Institute, National University of  
12 Singapore, Singapore

13 <sup>6</sup>Department of Biochemistry, Yong Loo Lin School of Medicine, National University of Singapore,  
14 Singapore

15 <sup>7</sup>Donald Danforth Plant Science Center, St. Louis, Missouri, USA

16 <sup>8</sup>USDA-ARS, Plant Genetics Research Institute, St. Louis, Missouri, USA

17 <sup>8</sup>GERMS and Infectious Disease Group, Genome Institute of Singapore, Singapore

18 <sup>9</sup>Division of Infectious Diseases, Department of Medicine, Yong Loo Lin School of Medicine,  
19 National University of Singapore, Singapore

20 <sup>10</sup>Department of Chemistry, National University of Singapore, Singapore

21 <sup>11</sup>Department of Microbiology and Molecular Medicine, University of Geneva, Switzerland

22 #Contributed equally

23 \*Corresponding author

24 **Email:** kimberly.kline@unige.ch

25 RR: <https://orcid.org/0000-0003-0737-9116>

26 ZJN: <https://orcid.org/0000-0001-9662-4958>

27 KK: <http://orcid.org/0000-0002-5472-3074>

28 ACG: <https://orcid.org/0000-0002-3050-634X>

29

30

31

32

### 33 **Classification**

34 Biochemistry; microbiology

### 35 **Keywords**

36 Multiple peptide resistance factor (MprF), lysyl-phosphatidylglycerol (L-PG), cationic antimicrobial  
37 peptides (CAMPs), lipid homeostasis, lipid metabolism, adaptive remodeling

### 38 **Author Contributions**

39 Conceptualization: RR, ZJN, KAK

40 Formal analysis: RR, ZJN, DMHC, KKLC, ACG, SLC, SSC

41 Funding acquisition: MRW, KAK

42 Investigation: RR, ZJN, DMHC, KKLC, ACG, SLC

43 Methodology: RR, ZJN, DMHC, KKLC, ACG, SLC, SSC, SAM, DKA

44 Project administration: RR, ZJN, KAK

45 Supervision: RR, MRW, KAK

46 Writing – original draft: RR, ZJN, KAK

47 Writing – review & editing: RR, ZJN, DMHC, KKLC, ACG, SLC, SSC, MRW, KAK

### 48 **This PDF file includes:**

49 Main Text

50 Figures 1 to 8

51 Graphical Abstract

52

### 53 **Abstract**

54 The bacterial cell membrane is an interface for cell envelope synthesis, protein secretion,  
55 virulence factor assembly and a target for host cationic antimicrobial peptides (CAMPs). To resist  
56 CAMP killing, several Gram-positive pathogens encode the multiple peptide resistance factor  
57 (MprF) enzyme that covalently attaches cationic amino acids to anionic phospholipids in the cell  
58 membrane. While *E. faecalis* encodes two *mprF* paralogs, MprF2 plays a dominant role in  
59 conferring resistance to killing by the CAMP human  $\beta$ -defensin 2 (hBD-2) in *E. faecalis* strain  
60 OG1RF. The goal of the current study is to understand the broader lipidomic and functional roles  
61 of *E. faecalis mprF*. We analyzed the lipid profiles of parental wild type and *mprF* mutant strains  
62 and show that while  $\Delta mprF2$  and  $\Delta mprF1 \Delta mprF2$  mutants completely lacked cationic lysyl-  
63 phosphatidylglycerol (L-PG), the  $\Delta mprF1$  mutant synthesized ~70% of L-PG compared to the  
64 parent. Unexpectedly, we also observed a significant reduction of PG in  $\Delta mprF2$  and  $\Delta mprF1$   
65  $\Delta mprF2$ . In the *mprF* mutants, particularly  $\Delta mprF1 \Delta mprF2$ , the decrease in L-PG and PG is  
66 compensated by an increase in the phosphorus-containing lipid, GPDGDAG, and D-ala-  
67 GPDGDAG. These changes were accompanied by a downregulation of *de novo* fatty acid  
68 biosynthesis and an accumulation of long-chain acyl-acyl carrier proteins (long-chain acyl-ACPs),  
69 suggesting that the suppression of fatty acid biosynthesis was mediated by the transcriptional  
70 repressor FabT. Growth in chemically defined media lacking fatty acids revealed severe growth  
71 defects in the  $\Delta mprF1 \Delta mprF2$  mutant strain, but not the single mutants, which was partially  
72 rescued through supplementation with palmitic and stearic acids. Changes in lipid homeostasis  
73 correlated with lower membrane fluidity, impaired protein secretion, and increased biofilm  
74 formation in both  $\Delta mprF2$  and  $\Delta mprF1 \Delta mprF2$ , compared to wild type and  $\Delta mprF1$ . Collectively,

75 our findings reveal a previously unappreciated role for *mprF* in global lipid regulation and cellular  
76 physiology, which could facilitate the development of novel therapeutics targeting MprF.

## 77 **Significance Statement**

78 The cell membrane plays a pivotal role in protecting bacteria against external threats, such as  
79 antibiotics. Cationic phospholipids such as lysyl-phosphatidylglycerol (L-PG) resist the action of  
80 cationic antimicrobial peptides through electrostatic repulsion. Here we demonstrate that L-PG  
81 depletion has several unexpected consequences in *Enterococcus faecalis*, including a reduction  
82 of phosphatidylglycerol (PG), enrichment of a phosphorus-containing lipid, reduced fatty acid  
83 synthesis accompanied by an accumulation of long-chain acyl-acyl carrier proteins (long chain  
84 acyl-ACPs), lower membrane fluidity, and impaired secretion. These changes are not deleterious  
85 to the organism as long as exogenous fatty acids are available for uptake from the culture  
86 medium. Our findings suggest an adaptive mechanism involving compensatory changes across  
87 the entire lipidome upon removal of a single phospholipid modification. Such adaptations must be  
88 considered when devising antimicrobial strategies that target membrane lipids.

89

## 90 **Main Text**

91

### 92 **Introduction**

93

94 *Enterococcus faecalis* is a Gram-positive commensal bacterium that naturally inhabits the harsh  
95 environment of the human gastrointestinal tract. The Enterococci are amongst the most clinically  
96 significant nosocomial pathogens and cause a variety of opportunistic infections in susceptible  
97 individuals, including endocarditis, urinary tract infections, bacteremia, and wound infections (1).  
98 Complicating the management of these infections is the fact that Enterococci are naturally  
99 resistant to conventional antibiotics like aminoglycosides; have rapidly evolved resistance to other  
100 drugs like chloramphenicol, erythromycin, tetracyclines, and vancomycin (2); and readily form  
101 biofilm during infection, conferring phenotypic antibiotic tolerance on these organisms (3).

102

103 For Enterococci to successfully colonize their human hosts, they must resist the bactericidal  
104 effect of cationic antimicrobial peptides (CAMPs), amphipathic molecules that are part of the  
105 innate immune response against microbes during infection (4). CAMPs are produced by a wide  
106 range of organisms, including bacteria, fungi, plants, and animals, and exert their antibacterial  
107 effects via disruption of the cell membrane (5). In humans, CAMPs are divided into two main  
108 classes, the defensins, e.g., human neutrophil peptides (HNP) and human  $\beta$ -defensins (hBD),  
109 and the cathelicidins, e.g., LL-37 (6, 7). The positively charged moiety of CAMPs binds to  
110 negatively charged membrane phospholipid headgroups, whereas the hydrophobic moiety binds  
111 to hydrophobic regions created by phospholipid acyl chains. Bacterial cell death results from  
112 physical disruption of the membrane, for which three different models (barrel-stave, toroidal, and  
113 carpet) have been described (reviewed in (8)). More recently, a new mechanism of disruption in  
114 which CAMPs delocalize membrane lipids and proteins has been reported for some bacteria (8,  
115 9).

116

117 In *E. faecalis*, CAMPs are thought to target phosphatidylglycerol (PG), an anionic phospholipid  
118 which constitutes a major portion of the cell membrane (10, 11). To evade CAMP killing, Gram-  
119 positive bacteria have evolved mechanisms to modify their anionic phospholipids (9, 12-14). For  
120 example, esterification of PG with the cationic amino acid lysine enables *Staphylococcus aureus*  
121 to resist the killing action of CAMPs through electrostatic repulsion. This lysinylation of PG  
122 changes its net charge from negative to positive. Because this modification confers resistance to  
123 multiple CAMPs, the gene responsible was named *mprF* for multiple peptide resistance factor.  
124 MprF contains two domains that perform distinct enzymatic functions: a synthase domain  
125 responsible for modifying PG with amino acids (e.g., lysine), and a flippase domain responsible  
126 for transferring modified PG from the inner leaflet to the outer leaflet of the cytoplasmic

127 membrane (15). MprF has since been shown to confer protection against CAMPs in several other  
128 Gram-positive organisms including *Bacillus anthracis*, *Bacillus subtilis*, *E. faecalis*, *Listeria*  
129 *monocytogenes*, *Mycobacterium tuberculosis*, as well as in Gram-negative *Pseudomonas*  
130 *aeruginosa* (9, 12-14, 16-18).

131  
132 We previously showed that MprF2 confers resistance to killing by the CAMP human  $\beta$ -defensin 2  
133 (hBD-2) in *E. faecalis* strain OG1RF (9). Our findings are consistent with an earlier study which  
134 showed that deleting the *mprF2* gene in *E. faecalis* 12030 resulted in loss of L-PG and higher  
135 sensitivity to the CAMPs colistin, nisin, HBD-3, and polymyxin B (14). In OG1RF where selected  
136 phospholipid synthesis genes (including *mprF2*) were deleted, exogenous fatty acid  
137 supplementation resulted in tolerance to the cationic antibiotic daptomycin and changes in lipid  
138 composition (19). Mutations in genes encoding the LiaFSR 3-component system and  
139 phospholipid metabolism enzymes accompanied alterations in phospholipid composition in  
140 daptomycin-resistant strains of *E. faecalis* (20, 21). Such adaptive lipid remodeling also occurs in  
141 other bacterial species in response to environmental changes (22) and phospholipase activity  
142 (23).

143  
144 Our previous work and the above literature linking *mprF* genetic perturbation with cationic  
145 antimicrobial resistance and lipidomic alterations suggest a gap in knowledge about how *mprF*  
146 brings about such adaptive lipid remodeling. Thus, we sought to more thoroughly investigate the  
147 mechanism by which *mprF* affects lipid homeostasis in *E. faecalis*. Using lipidomic methods that  
148 we had previously established (24), we quantified lipids across various classes in wild type  
149 OG1RF and the  $\Delta mprF1$ ,  $\Delta mprF2$ , and  $\Delta mprF1 \Delta mprF2$  mutant strains. Coupled with  
150 transcriptomic analyses, gas chromatography analysis of total fatty acid methyl esters (GC-  
151 FAME), assays for membrane fluidity, secretion, biofilm formation, and CAMP susceptibility, we  
152 have discovered a previously unappreciated role for *mprF* in global lipid regulation and cellular  
153 physiology.

## 154 155 Results

### 156 157 *mprF* deletion alters levels of membrane phospholipids

158 We previously observed that human  $\beta$ -defensin 2 (hBD-2) binds *E. faecalis* more strongly at foci  
159 situated at or near the division septum in the  $\Delta mprF2$  mutant than in the wild type, and that only  
160 MprF2, and not MprF1, protects against hBD-2-mediated killing (9). The  $\Delta mprF2$  strain is also more  
161 susceptible to LL-37, a cathelicidin that is more potent than hBD2, compared to the  $\Delta mprF1$  strain,  
162 and  $\Delta mprF1 \Delta mprF2$  is significantly more susceptible to hBD-2 than  $\Delta mprF1$  (but not  $\Delta mprF2$ ) at  
163 50  $\mu\text{g/ml}$  (**Fig. S1A, S1B**). We hypothesized that differences in CAMP susceptibility between *mprF1*  
164 and *mprF2* mutants may be due to differences in levels of aminoacylated lipids. Previously, we  
165 performed untargeted lipidomics to identify the phospholipid and glycolipid repertoire of *E. faecalis*  
166 OG1RF, and multiple reaction monitoring (MRM) to quantify phosphatidylglycerol (PG) and lysyl-  
167 PG (L-PG) molecules in this strain and in two daptomycin-resistant strains (10). In the current study,  
168 we used the same methodology to compare the levels of L-PG in  $\Delta mprF1$ ,  $\Delta mprF2$ , and  $\Delta mprF1$   
169  $\Delta mprF2$  mutants with the parental wild type strain. We found that  $\Delta mprF2$  and  $\Delta mprF1 \Delta mprF2$   
170 cells had no detectable L-PG (**Fig. 1A, S1C**), as previously described by Bao and colleagues (14),  
171 whereas total L-PG was present in the  $\Delta mprF1$  mutant at 70% of the wild type level. Unlike previous  
172 thin layer chromatography (TLC) studies which lacked the sensitivity to discriminate between  
173 individual lipid molecules and quantify their levels, using LC-MS/MS we were able to observe that  
174 MprF1 also contributes to L-PG synthesis in *E. faecalis* OG1RF under these laboratory conditions.

175  
176 To determine whether the above differences in L-PG levels were due to differential *mprF* gene  
177 expression, we performed quantitative reverse transcription polymerase chain reaction (RT-qPCR)  
178 of the *mprF* paralogs in the wild type. RT-qPCR revealed that *mprF2* expression is 200-fold higher  
179 than *mprF1* expression (**Fig. S2A**). This differential expression would explain MprF1's relatively

180 minor contribution to L-PG production. We also observed that deleting either *mprF* paralog does  
181 not affect the expression of the remaining paralog (**Fig. S2B**).

182

183 As L-PG synthesis requires PG as a substrate, we predicted that PG levels would be higher in  
184 mutants unable to convert a fraction of PG to L-PG. Unexpectedly,  $\Delta mprF2$  and  $\Delta mprF1 \Delta mprF2$   
185 mutants had significantly less PG than wild type. Moreover, similar to our observation for L-PG,  
186  $\Delta mprF1$  also had an intermediate amount of PG compared to wild type and the other two *mprF*  
187 mutants (**Fig. 1B, S1D**). The reduction in PG was unexpected because its biosynthetic gene (*pgsA*)  
188 is thought to be essential in *E. faecalis*, based on the fact that this gene is essential in many other  
189 bacterial species (25). However, our mutants do not show any growth defect (**Fig. S2C**), change in  
190 viability (**Fig. S2D**), or increased membrane permeability to propidium iodide (**Fig. S2E**).

191

192 Complementing the  $\Delta mprF2$  mutant with *mprF2* on a plasmid more than restored L-PG to wild type  
193 levels (**Fig. 1A, S3A**) and partially restored PG levels (**Fig. 1B, S3B**), the latter possibly being the  
194 result of the complemented strain producing more L-PG than the wild type and therefore depleting  
195 the PG precursor. When the double mutant was complemented with the *mprF2* gene, L-PG was  
196 restored to wild type levels, whereas the level of PG was lower than in the uncomplemented double  
197 mutant (**Fig. 1A, 1B**). To confirm that it is MprF2's enzymatic activity in L-PG production (rather  
198 than another indirect effect of MprF2) that determines PG levels, we complemented the  $\Delta mprF2$   
199 mutant with inactive *mprF2* on a plasmid. This complementation failed to restore L-PG to wild type  
200 levels (**Fig. S1E, S1G**). The catalytically inactive *mprF2* possesses mutations in residues  
201 coordinating its interaction with the aminoacyl moiety of lys-tRNA at similar locations (D739A,  
202 R742S) as previously described in *B. licheniformis* (26). Inactive *mprF2* complementation also  
203 failed to restore PG to levels achieved through complementation with native MprF2 (**Fig. S1F**,  
204 **S1H**).

205

206 We also considered the individual effects of each paralog's N-terminal flippase and C-terminal  
207 catalytic domains on L-PG and PG levels. Complementation with both domains of *mprF2* is required  
208 for L-PG production (**Fig. S3A**). Restoration of L-PG and PG levels was not possible through  
209 complementation with either full length *mprF1* or individual domains of either paralog. (**Fig. S3A-**  
210 **D**).

211

212 Collectively, our results suggest that deletion of *mprF1*, *mprF2*, or both genes causes more  
213 widespread changes in phospholipid homeostasis than previously appreciated.

214

#### 215 ***mprF* deletion affects lipids in other classes**

216 In light of reduced L-PG and PG in the *mprF* mutants and the fact that PG is an essential lipid in  
217 many Gram-positive bacteria (27-29), we hypothesized that the mutants might adjust the  
218 abundances of other lipid classes via adaptive lipidome remodeling (22) to compensate for the  
219 depletion of otherwise essential lipids. We first conducted one-dimension thin layer  
220 chromatography (1D-TLC) of lipid extracts of each strain, using <sup>14</sup>C radiolabeling and iodine  
221 staining (**Fig. 2A**). Six major spots were observed in the 1D-TLC which were identified as  
222 diglucosyl-diacylglycerol (DGDAG), L-PG, glycerophospho-diglucosyl-diacylglycerol (GPDGDAG),  
223 D-ala-GPDGDAG, PG and cardiolipin (CL) co-migrating in a single spot, and a spot of unknown  
224 identity containing phosphorus (**Fig. 2A**). Identities of each spot were determined by a combination  
225 of 1- and 2-dimension TLC analyses with lipid standards, ninhydrin staining, mass spectrometry,  
226 and <sup>32</sup>P and <sup>14</sup>C radiolabeling as described in **Supplementary Text 1A**.

227

228 Both the <sup>14</sup>C radiolabeled and iodine-stained TLC plates indicate that L-PG is lower only in  $\Delta mprF2$   
229 and  $\Delta mprF1 \Delta mprF2$  and that reduction was restored by complementation with *pmprF2*-HA (**Fig.**  
230 **2A**), findings which corroborate the quantification data obtained via LC-MS/MS-based multiple  
231 reaction monitoring (**Fig. 1A**). We observed more intense spots of GPDGDAG and D-ala-  
232 GPDGDAG in these mutants compared to wild type, although the difference was not statistically  
233 significant. Combined PG and CL spot intensities were unchanged across the different mutants.

234 We also observed stronger spot intensities for the phosphorus-containing lipid of unknown identity  
235 in  $\Delta mprF2$  and  $\Delta mprF1 \Delta mprF2$  (**Fig. 2B**). Although we have yet to identify this lipid, TLC analysis  
236 confirmed that the spot is a lipid (positive iodine staining and presence of fatty acyl product ions  
237 from MS2 analysis) that contain phosphorus (positive  $^{32}\text{P}$  radiolabeling) but no amino groups  
238 (negative ninhydrin staining) (**Fig. 2B, S4C-E**). Based on MS analysis, this unknown lipid spot  
239 contains 18 species that do not belong to any of the lipid classes we have previously studied (i.e.  
240 PG, LPG, Ala-PG, Arg-PG, DGDAG, MGDAG, GPDGDAG). MS-MS analysis of the precursor ions  
241 reveals that they contain fatty acyl chains and three common products ions ( $m/z$ : 379.1, 397.1,  
242 415.1) that were consistent across all species, suggesting that these species belong to the same  
243 class (**Supplementary Excel Table S1C**). Complementation with  $pmpF2$ -HA restored this lipid to  
244 wild type levels (**Fig. 2A**).

245  
246 As PG is a substrate for GPDGDAG synthesis (30), we asked whether GPDGDAG levels were  
247 significantly altered in mutants where PG was reduced.  $^{14}\text{C}$ -radiolabeled TLC revealed faint spots  
248 for GPDGDAG. Since it was not possible to discern any differences in GPDGDAG levels via TLC  
249 (**Fig. 2B**), we performed a semi-quantitative mass spectrometric analysis on one particular  
250 GPDGDAG species, GPDGDAG 34:1 (**Fig. 2C**) that we previously determined to be the most  
251 abundant species within the class (10). By this latter analysis,  $\Delta mprF1 \Delta mprF2$  showed a 5-fold  
252 increase in GPDGDAG 34:1 levels relative to wild type, with  $\Delta mprF1$  and  $\Delta mprF2$  showing 2- and  
253 4-fold higher GPDGDAG 34:1 levels, respectively (**Fig. 2C**). Absolute quantification via MRMs was  
254 not possible due the lack of a commercially available standard.

255  
256 Since GPDGDAG 34:1 was higher in the  $mprF$  mutants, we considered whether the abundance of  
257 its downstream product, lipoteichoic acid (LTA) (which is poly-glycerophosphate polymerized onto  
258 a GPDGDAG membrane anchor) might be affected as well (31). However, immunoblots of whole  
259 cell lysates and supernatants from the wild type and  $mprF$  mutants revealed no difference in LTA  
260 levels in the whole cell lysates, and no shed LTA in the supernatants of any strain, suggesting that  
261 LTA levels remain unchanged in these mutant backgrounds (**Fig. S1I**).

262  
263 Due to the lack of a commercially available DGDAG standard, we performed semi-quantitative  
264 MRMs for DGDAG using a monoglucosyl-diacylglycerol (MGDAG) surrogate standard (**Fig. 2D**).  
265  $\Delta mprF1$  and  $\Delta mprF2$  had more total DGDAG than the wild type, while DGDAG in  $\Delta mprF1 \Delta mprF2$   
266 was at the wild type level (**Fig. 2D**). The same trend was observed for most of the individual DGDAG  
267 species (**Fig. S1J**).

268  
269 To discriminate between individual PG and CL spot intensities, we performed 2D TLCs to further  
270 separate the co-migrating PG and CL spots in the first dimension (**Fig. 2E**). We observed that the  
271 PG spot intensity was slightly lower in  $\Delta mprF1 \Delta mprF2$  while CL appears unchanged (**Fig. 2F**).  
272 Similar to the 1D-TLCs, L-PG appeared to be lower while the unknown phosphorus-containing lipid  
273 spot, together with the D-ala-GPDGDAG and GPDGDAG spots, appeared stronger in intensity in  
274  $\Delta mprF1 \Delta mprF2$  (**Fig. 2F**). However, DGDAG was stained more intensely (**Fig. 2E, 2F**) unlike what  
275 was observed in the MS analysis (**Fig. 2C**). This difference could be due to another  $^{14}\text{C}$ -  
276 radiolabeled compound co-migrating with DGDAG, resulting in more intensely stained 2D- and 1D-  
277 TLCs (though the staining intensity difference is not statistically significant) (**Fig. 2B, 2F**). All of  
278 these observations suggest that in the  $mprF$  mutants, particularly  $\Delta mprF1 \Delta mprF2$ , the decrease  
279 in L-PG and PG is compensated by an increase in the phosphorus-containing lipid, GPDGDAG,  
280 and D-ala-GPDGDAG.

## 281 282 ***mprF* deletion results in decreased expression of fatty acid synthesis genes**

283 Since  $mprF$  deletion resulted in alterations in phospholipid and glycolipid levels, we hypothesized  
284 that these altered levels might be due to altered expression of genes involved in lipid metabolism.  
285 To test this hypothesis, we performed RNA sequencing to compare the gene expression profiles of  
286 the wild type and the  $mprF$  mutants. In total, 301 genes (14% of the genome) were differentially  
287 expressed between the wild type and  $\Delta mprF1 \Delta mprF2$  (**Fig. S5A**). Principal component analysis

288 revealed that the transcriptomic profile of  $\Delta mprF2$  clusters more closely to that of  $\Delta mprF1 \Delta mprF2$ ,  
289 suggesting that *mprF2* deletion is associated with more transcriptional changes than *mprF1*  
290 deletion (**Fig. S5B**). A Venn diagram of genes differentially expressed in the *mprF* mutants relative  
291 to wild type indicates that *mprF1* and *mprF2* have individual effects that are amplified in the double  
292 mutant, from which we infer that the mutant phenotypes are not only due to epistasis (**Fig. S5C**).  
293 We performed a statistical analysis of gene sets in all four strains and, consistent with our  
294 hypothesis, we found downregulation of nine genes associated with fatty acid metabolism and  
295 biosynthesis in  $\Delta mprF1 \Delta mprF2$  (**Fig. 3A, B**). Genes involved in the initiation, elongation, and  
296 termination phases of fatty acid synthesis (*accA*, *accB*, *accC*, *accD*, *fabD*, *fabF2*, *fabG3*, *fabK*, and  
297 *fabZ2*) were downregulated in the double mutant (**Fig. 3B, S5A**). Using RT-qPCR, we confirmed  
298 that genes encoding components of the *de novo* fatty acid biosynthesis pathway were  
299 downregulated in the double mutant. By contrast, expression of the essential gene *pgsA*, which  
300 encodes an enzyme involved in PG synthesis, was slightly upregulated in the double mutant (**Fig.**  
301 **S5D**), perhaps in an attempt to compensate for the decrease in the levels of PG.

302

### 303 **Saturated fatty acids restore *mprF* growth in nutrient-limited media**

304 Since *de novo* fatty acid biosynthesis is downregulated in  $\Delta mprF1 \Delta mprF2$ , we speculated that this  
305 mutant might require exogenous fatty acids for growth and survival. *E. faecalis* can incorporate  
306 exogenous fatty acids into its membrane when grown in bovine heart infusion (BHI) culture medium  
307 (32). We performed a gas chromatography analysis of total fatty acid methyl esters (GC-FAME) on  
308 BHI, in which we detected only two fatty acids - palmitic (C<sub>16:0</sub>) and stearic acid (C<sub>18:0</sub>)  
309 (**Supplementary Excel Table S1D**). We thus hypothesized that  $\Delta mprF1 \Delta mprF2$  takes up these  
310 fatty acids from BHI to counteract the downregulation of *de novo* fatty acid biosynthetic genes. As  
311 expected, we observed that growth of the double mutant was severely impaired in nutrient-limited,  
312 chemically defined media (CDM) lacking fatty acids, while growth of the single mutants was less  
313 severely impaired (**Fig. 4A**). Supplementing CDM with either palmitic acid (**Fig. 4B, S6A**) or stearic  
314 acid (**Fig. 4C, S6B**) promoted growth of both strains at all concentrations  $\geq 31.25$  ng/ml. A 3:1 mix  
315 of palmitic and stearic acid mimicking the ratios at which they are present in BHI (**Supplementary**  
316 **Excel Table S1D**) promoted growth of the double mutant up to 125 ng/ml. The mix promoted growth  
317 of the wild type at all concentrations (**Fig. S6C, D**). Unsaturated fatty acids at a concentration of 5  
318  $\mu$ g/ml inhibited growth of both strains (**Fig. S6E, F**). Of the other saturated fatty acids (myristic,  
319 lauric, and arachidic acids), only arachidic acid promoted growth of both strains at all concentrations  
320 (**Fig. S6G, H, I**). Collectively, our findings suggest that the *mprF* null mutant relies on exogenous  
321 palmitic acid and stearic acid for survival when *de novo* fatty acid biosynthesis is downregulated.

322

### 323 **L-PG depletion increases the proportion of long chain acyl-ACPs in the double mutant**

324

325 *Lactococcus lactis* uses the MarR (multiple antibiotic resistance repressor) family repressor FabT  
326 to regulate expression of the *fab* gene operon (33). FabT binds to regulatory elements of the FA  
327 biosynthesis operon to repress transcription of *fab* genes in *Streptococcus pneumoniae* (34).  
328 However, in *S. pneumoniae*, FabT binds DNA only when complexed with acyl-acyl carrier protein  
329 (acyl-ACP) species that have long-chain acyl moieties (35). Acyl carrier proteins (ACPs) play  
330 essential roles in fatty acid synthesis as well as phospholipid synthesis by mediating the transfer of  
331 long fatty acyl chains from fatty acids to glycerol 3-phosphate (36, 37). *E. faecalis* FabT is 51%  
332 identical to that of *S. pneumoniae* and functions in a similar manner to *S. pneumoniae* FabT (38).  
333 Thus, we hypothesized that L-PG depletion in the double mutant leads to an accumulation of long-  
334 chain fatty acyl-ACPs, which would increase FabT affinity for the *fab* promoter, resulting in the  
335 observed suppression of *de novo* FA biosynthesis and increased dependence on exogenous fatty  
336 acids. To measure acyl-ACP levels within our strains, we took advantage of an Asp-N protease to  
337 cleave at a conserved DSLD amino acid sequence present at the acyl attachment site, leaving  
338 behind a DSL peptide connected to 4'-phosphopantetheine and an acyl-group which is then  
339 detected using mass spectrometry. The conserved nature of the Asp-N cleavage site and  
340 consistent structure of the digestion products makes quantification of acyl-ACP species possible  
341 (39, 40). *E. faecalis* contains two *acp* genes, *acpA* and *acpB*. However, only AcpA – the ACP that

342 is involved in *de novo* fatty FA biosynthesis – possesses the conserved DSLD sequence, while  
343 AcpB – the ACP involved in uptake of exogenous fatty acids – does not (38). Thus, this method  
344 would preferentially detect acyl-AcpA species. We observed that the double mutant contains higher  
345 proportions of acyl-AcpA species containing 10 to 18 carbon atoms than the wild type with a notable  
346 decrease in acyl-AcpA species with 2 carbon atoms (**Fig. 5, S7A**). These data confirm the  
347 hypothesis that long-chain fatty acyl-ACPs accumulate in the double mutant and provide  
348 mechanistic insight for how changes in MprF can impact global lipid homeostasis in the cell.  
349

### 350 **Fatty acid profiles are altered in *mprF* mutants**

351 Given the downregulation of *de novo* fatty acid biosynthesis genes in  $\Delta mprF1 \Delta mprF2$  and the  
352 ability of exogenous fatty acids to support this mutant's growth in CDM, it was expected that the  
353 fatty acid profile of the double mutant differs from that of the wild type in the two different media  
354 (BHI and CDM). Gas chromatography analysis of total fatty acid methyl esters (GC-FAME) was  
355 performed on lyophilized cell pellets of the wild type and  $\Delta mprF1 \Delta mprF2$  grown in either BHI or  
356 CDM. The fatty acid profiles of the wild type and  $\Delta mprF1 \Delta mprF2$  grown in BHI were very similar  
357 (**Fig. 6, Supplementary Excel Table S1E**). However, when grown in CDM,  $\Delta mprF1 \Delta mprF2$  had  
358 11% more palmitic acid ( $C_{16:0}$ ), ~11% less *cis*-vaccenic acid ( $C_{18:1 \omega 7 \text{ cis}}$ ), and ~2.5% less  $C_{19 \text{ cyclo } \omega 7}$   
359 acid relative to the wild type, whereas the wild type showed a decrease of 2% and 3% in palmitic  
360 acid ( $C_{16:0}$ ) and stearic acid ( $C_{18:0}$ ), respectively, and a ~6% increase in *cis*-vaccenic acid ( $C_{18:1 \omega 7 \text{ cis}}$ )  
361 compared to growth in BHI (**Fig. 6, Supplementary Excel Table S1E**).  $\Delta mprF1 \Delta mprF2$  grown  
362 in CDM showed a ~11% increase in palmitic acid ( $C_{16:0}$ ), a ~7% decrease in *cis*-vaccenic acid ( $C_{18:1 \omega 7 \text{ cis}}$ )  
363 and a ~3.5% decrease in  $C_{19 \text{ cyclo } \omega 7}$  relative to growth in BHI (**Fig. 6, Supplementary Excel**  
364 **Table S1E**). Collectively, these results suggest that the  $\Delta mprF1 \Delta mprF2$  fatty acid composition  
365 differs from that of the wild type, in a growth medium-dependent manner. Wild type *E. faecalis*  
366 makes less  $C_{16:0}$  and more  $C_{18:1 \omega 7 \text{ cis}}$  in CDM while  $\Delta mprF1 \Delta mprF2$  makes more  $C_{16:0}$  and less  $C_{18:1 \omega 7 \text{ cis}}$   
367 in CDM. These fatty acid differences could be the cause, or the effect, of the double mutant's  
368 severely impaired growth in CDM.  
369

### 370 ***mprF* deletion has multiple functional consequences**

371  
372 We hypothesized that extensive lipidomic and transcriptomic alterations in the absence of *mprF*  
373 would affect cell physiology. Below we describe multiple functional changes that we observed in  
374 the *mprF* mutants.  
375

#### 376 *Secretion*

377 Anionic membrane phospholipids promote efficient secretion via the generalized Sec pathway (41,  
378 42). Therefore, we hypothesized that lower PG levels in the *mprF* mutants would impair secretion.  
379 To test this hypothesis, we compared the secretion efficiency of wild type with that of the single and  
380 double *mprF* mutants. We observed reduced bulk secretion in the *mprF* mutants with the greatest  
381 decrease observed for  $\Delta mprF1 \Delta mprF2$ , followed by  $\Delta mprF2$  and  $\Delta mprF1$  (**Fig. 7A**). To validate  
382 the disruption of Sec-mediated secretion, a chimeric alkaline phosphatase was heterologously  
383 expressed in wild type and the *mprF* mutants and its secretion into the supernatant detected  
384 colorimetrically. Relative to wild type, the *mprF* mutants displayed significant impairment in  
385 secretion, with  $\Delta mprF1 \Delta mprF2$  showing the greatest secretion defect (**Fig. 7B**).  
386

#### 387 *Membrane fluidity*

388 The fluidity of the cell membrane is influenced by the amount of unsaturated lipids present, where  
389 a higher degree of unsaturation results in more fluid membranes (43). Based on the reduction of  
390 unsaturated L-PG in the *mprF* mutants (**Fig. 2, S1C**) and alterations in other lipid classes, we  
391 hypothesized that membrane fluidity might be affected as well. Membrane fluidity was assayed  
392 using a fluorescent dye sensitive to fluidity changes, Laurdan. Laurdan inserts into membrane  
393 bilayers and, depending on how liquid ordered ( $L_o$ ) or disordered ( $L_d$ ) the local lipid environment is,  
394 its emission spectra will blue-shift (in  $L_o$  regions) or red-shift (in  $L_d$  regions) respectively (44, 45).  
395 This spectral shift can be detected by measuring the green and blue wavelengths and expressing



396 the readings as a ratio, generalized polarization (GP), where higher GP values imply more rigid  
397 membranes and lower GP values imply more fluid membranes. By staining late stationary phase  
398 cultures of the wild type and *mprF* mutants with Laurdan and imaging cells by microscopy, we  
399 observed that  $\Delta mprF2$  and  $\Delta mprF1 \Delta mprF2$  had higher GP values, indicating slightly more rigid  
400 membranes in these mutants compared to the wild type, while  $\Delta mprF1$  had no significant difference  
401 in GP values (**Fig. 7C**). Hence, the lipidomic changes observed in  $\Delta mprF1 \Delta mprF2$  are correlated  
402 with lower membrane fluidity.

403

#### 404 *Biofilm formation*

405 In *E. faecalis* strain 12030, the loss of *mprF* enhances biofilm formation (14). To determine whether  
406 loss of *mprF* has the same effect in strain OG1RF, we used crystal violet staining to assay biofilm  
407 formation from wild type and *mprF* mutants grown in microtiter plates. The stain detects adherent  
408 biomass. We observed slight increases in biofilm formation for the  $\Delta mprF1$  and  $\Delta mprF2$  mutants,  
409 with the increase being significant for  $\Delta mprF1 \Delta mprF2$  ( $P \leq 0.001$ ) across all daily timepoints over  
410 a 5-day period (**Fig. 7D**).

411

#### 412 **Discussion**

413

414 The major conclusion of this study is that depletion of a cationic membrane phospholipid (L-PG)  
415 leads to unexpected lipidomic, transcriptomic, and functional changes in *E. faecalis*, and that the  
416 two MprF paralogs of *E. faecalis* contribute differently to the observed changes. Specifically,  
417 MprF2 is not only more important for protection against CAMP-mediated killing than MprF1, but is  
418 also involved in global lipid homeostasis and cell function.

419

420 In the current study, we used previously established mass spectrometry-based methods (10) to  
421 analyze various lipids in *E. faecalis* OG1RF,  $\Delta mprF1$ ,  $\Delta mprF2$ , and  $\Delta mprF1 \Delta mprF2$ . One  
422 advantage of such methods is that they are much more sensitive than traditional thin layer  
423 chromatography (TLC), enabling a more comprehensive understanding of lipid homeostatic shifts  
424 that are dependent upon *mprF* (14). When we compared the lipid compositions of *mprF* deletion  
425 mutants with the parent OG1RF strain, we found that, as expected, deletion of *mprF2* resulted in  
426 a complete absence of L-PG from the membrane. The observed absence of L-PG in  $\Delta mprF2$  is  
427 consistent with our previous work showing that  $\Delta mprF2$  is significantly more sensitive to killing by  
428 human  $\beta$ -defensin 2 (hBD2) than  $\Delta mprF1$  (9). Unlike previous reports, however, we found that  
429 *mprF1* also contributes to L-PG production in *E. faecalis*, a key phenotypic difference that  
430 motivated us to explore changes elsewhere in the *E. faecalis* lipidome. While we observed that L-  
431 PG is only slightly reduced in  $\Delta mprF1$  (*mprF2* present), L-PG is completely absent in  $\Delta mprF2$   
432 (*mprF1* present). The unexpected observation that MprF1 alone does not synthesize L-PG  
433 suggests that MprF2 expression is necessary for MprF1 to function. This possibility warrants  
434 further investigation.

435

436 To our surprise, we also discovered that  $\Delta mprF2$  and  $\Delta mprF1 \Delta mprF2$  have significantly lower PG  
437 levels than wild type and  $\Delta mprF1$ . This is a novel and unexpected finding because *mprF* acts  
438 downstream of *pgsA*, one of two genes (along with *pgpA*) involved in PG synthesis (**Fig. 8**).  
439 Concurrently, levels of GPDGDAG, D-ala-GPDGDAG, and a phosphorous-containing lipid  
440 increase, possibly a cellular response to compensate for the loss of PG and L-PG and maintain  
441 cell membrane integrity. DGDAG is a membrane lipid that serves as the lipid anchor of  
442 lipoteichoic acids (LTA) in Gram-positive bacteria. As the phosphoglycerol headgroup is  
443 consumed to form polymeric LTA, DAG accumulates in the membrane (30). It has been  
444 suggested that the consumption of phosphorous could be offset by an accumulation of DGDAG in  
445 *Staphylococcus haemolyticus* and *Staphylococcus epidermidis* (46). GPDGDAG is a glycolipid  
446 formed as an intermediate during synthesis of lipoteichoic acid (LTA) in *S. aureus* (47). A  
447 lipidomic comparison between daptomycin-resistant *E. faecalis* strain R712 and daptomycin-  
448 sensitive strain S613 revealed that R712 had less PG, L-PG, and CL than S613 but more MGDG  
449 and DGDG, and that this glycolipid upregulation is consistent with an increase in GPDGDAGs

450 reported earlier by another group (20, 48). Based on these earlier findings and our own results,  
451 we conclude that these phospholipids and glycolipids are linked by common pathways in *E.*  
452 *faecalis*. Additional experiments are needed to determine the identity of the phosphorus-  
453 containing lipid, and to fully understand the roles of it, along with DGDAG and GPDGDAG, in *E.*  
454 *faecalis* membrane homeostasis and function.

455  
456 We show that long-chain acyl-ACPs, precursors for phospholipid synthesis, accumulate in the  
457 absence of MprF, which we speculate is a consequence of the loss of major lipids such as PG  
458 and L-PG. These long-chain acyl-ACPs activate the transcriptional repressor FabT, which  
459 represses *de novo* fatty acid biosynthesis, resulting in increased dependence on exogenous fatty  
460 acids for growth. In *E. faecalis*, acyl-AcpA was recently shown to enhance FabT binding to DNA  
461 (49). We thus propose a model in which deletion of *mprF1* and *mprF2* mediates lipidomic and  
462 transcriptomic changes via enhanced FabT activity resulting from an accumulation of long-chain  
463 acyl-AcpA species (**Fig. 8**).

464  
465 As a consequence of these lipidomic and transcriptomic changes, the cells manifest a secretion  
466 defect, increased membrane rigidity, and enhanced CAMP binding. The secretion machinery of *B.*  
467 *subtilis* requires interfacial regions of high and low fluidity to function optimally (44). As membrane  
468 fluidity influences secretion, the impaired secretion that we observed in  $\Delta mprF1$ ,  $\Delta mprF2$ , and  
469  $\Delta mprF1\Delta mprF2$  is consistent with findings in *B. subtilis* as well as with earlier studies demonstrating  
470 that efficient secretion requires anionic phospholipids (41, 42, 50, 51). Another study which  
471 investigated factors governing *Listeria monocytogenes* secretion of listeriolysin demonstrated a  
472 secretion defect in an *mprF* mutant, further implicating MprF in bacterial secretion (52). Collectively,  
473 these observations support a model of efficient secretion requiring both modified anionic  
474 phospholipids and optimal membrane fluidity in *E. faecalis*.

475  
476 We previously reported that all L-PG species in laboratory-grown *E. faecalis* are unsaturated, i.e.  
477 they contain at least one carbon-carbon double bond in a constituent acyl chain (24). Here we  
478 show that all L-PG species are absent from  $\Delta mprF2$  and  $\Delta mprF1\Delta mprF2$ . As acyl chain  
479 unsaturation is correlated with membrane fluidity (53), our results suggest that the lower  
480 membrane fluidities of these two mutant strains are due to the lack of unsaturated L-PG species.  
481 Although the ratio of saturated-to-unsaturated acyl chains is similar for the wild type and the  
482 double mutant, a recent study suggests that acyl chain remodeling in different phospholipid  
483 classes affects membrane properties differently (22). In that study, out of 27 lipid species  
484 identified in *Methylobacterium extorquens*, as few as 8 were highly variable over all of the  
485 conditions tested (various temperatures, osmotic and detergent stresses, carbon sources, and  
486 cell densities). Thus, only a fraction of the lipidome was involved in adaptive remodeling. Different  
487 sets of lipidomic features (phospholipid class, acyl chain saturation, and acyl chain length) were  
488 involved in responses to changes in temperature, high salt concentrations, and stationary growth  
489 phase. One of the more striking observations was that varying the degree of acyl chain saturation  
490 in PE, PG, or phosphatidylcholine (PC) had varying effects on lipid packing, a property that is  
491 correlated with other physical properties including viscosity (54). Cells maintain optimal  
492 membrane properties when exposed to environmental challenges (e.g. changes in temperature,  
493 acidic pH, osmotic stress) through an adaptive response known as homeoviscous adaptation,  
494 which involves changes to the acyl chain composition of membrane lipids (55). Consistent with  
495 the *M. extorquens* study, our findings support the concept that lipid class-dependent acyl chain  
496 remodeling provides a mechanism by which to optimize the cell membrane's biophysical  
497 properties, thus greatly improving our understanding of membrane adaptation.

498  
499 In summary, our findings therefore suggest roles for MprF beyond mediating resistance to cationic  
500 antimicrobials via L-PG synthesis. Our study underscores the need to consider broader  
501 consequences of mutations involving lipid-related genes, as they may lead to unanticipated  
502 changes within other lipid classes as part of an adaptive response involving global lipid remodeling.  
503 Such adaptations need to be considered when devising novel antimicrobial strategies that target

504 membrane lipids. The lipidome remodeling we report here also underscores the importance of  
505 mass spectrometry-based lipidomics in understanding the behavior of one of the most clinically  
506 significant opportunistic pathogens.

507

## 508 **Materials and Methods**

509

510 Strains, growth conditions, RT-qPCR, growth kinetics, live/dead staining, RNA sequencing,  
511 cloning methods and methods for MS analysis of the TLC spots are detailed in the

512 **Supplementary Text 1B.**

513

### 514 **Analysis of membrane lipid content**

515 Lipids were extracted from lyophilized cell pellets from late stationary phase cultures using a  
516 modified Bligh & Dyer method in which the extraction solvent contained chloroform/methanol in a  
517 ratio of 1:2 (v/v) as previously described (10). For method validation and quantification, known  
518 amounts of internal standards for phosphatidylglycerol (PG) and lysyl-PG (L-PG) were added to  
519 the samples. Nine hundred microliters of chilled extraction solvent containing internal standards  
520 (Avanti polar lipids, Alabaster, AL, USA) was added to the dry cell pellets except monoglucosyl-  
521 diacylglycerol (MGDAG) 34:1 which was used as a surrogate external standard for diglucosyl-  
522 diacylglycerol (DGDAG) instead (**Table S1B**).

523

524 Lipid extraction was then carried out as previously described (10). The dried lipid extract was  
525 resuspended in a mixture of chloroform and methanol (1:1 v/v), to a final lipid concentration of 10  
526 mg/ml. This solution was stored at -80 °C until the mass spectrometry analysis was performed.  
527 PG and L-PG in *E. faecalis* were quantified by LC-MS/MS using multiple reaction monitoring  
528 (MRM) using a previously described methodology (10). An Agilent 6490 QqQ mass spectrometer  
529 connected to a 1290 series chromatographic system was used with a Kinetex® 2.6 µm HILIC  
530 column (100 Å, 150 x 2.1 mm) (Phenomenex, USA). Electrospray ionization (ESI) was used to  
531 ionize lipids. Each lipid molecular species was analyzed using a targeted multiple reaction  
532 monitoring (MRM) approach containing transitions for known precursor/product mass-to-charge  
533 ratio (m1/m3). Signal intensities were normalized to the spiked internal standards (PG 14:0 and L-  
534 PG 16:0) to obtain relative measurements and further normalized against the initial dry cell pellet  
535 weight, as described previously (10).

536

537 To determine the species of DGDAG present in *E. faecalis*, untargeted analysis of lipid extracts of  
538 WT,  $\Delta mprF1$ ,  $\Delta mprF2$  and  $\Delta mprF1 \Delta mprF2$  was carried out. Lipid extracts were analyzed using  
539 an Agilent 6550 QToF mass spectrometer connected to a 1290 series chromatographic system  
540 with a Kinetex® 2.6 µm HILIC column (100 Å, 150 x 2.1 mm) (Phenomenex, USA). The QToF  
541 instrument was set to positive ion mode, at an electrospray voltage of -3500 V (Vcap), a  
542 temperature of 200 °C, a drying gas rate of 14 L/min. Spectra were acquired in auto-MS2 mode  
543 with MS1 acquisition rate at 4 spectra/s and the MS2 acquisition rate at 20 spectra/s with fixed  
544 collision energy at 40 eV. The list of detected species of DGDAG in the samples can be found in  
545 the **Supplementary Excel Table S1A**.

546

547 Due to the absence of suitable internal standards, semi-quantitative analysis of DGDAG was  
548 carried out instead. Lipid extraction was performed as described above without addition of  
549 internal standards. Analysis of DGDAG lipid species was performed by LC-MS/MS via MRMs  
550 using monoglucosyl-diacylglycerol (MGDAG) 34:1 as a surrogate standard (**Table S1B**) for  
551 external calibration curves. Measurements of MGDAG 34:1 dilution from 0.2 ng/mL to 1000  
552 ng/mL were used to construct external calibration curves to estimate the levels of DGDAG.  
553 Estimated DGDAG levels were then normalized against dry cell pellet weight of the respective  
554 samples. The MRM transitions for DGDAG molecular species and MGDAG 34:1 are listed in  
555 **Supplementary Excel Table S1B**. The mobile phase gradients used for all experiments are as  
556 previously described (10). For semiquantitative analysis of glycerophosphoryl-diglucosyl-  
557 diacylglycerol (GPDGDAG), lipid extracts were analyzed using an Agilent 6550 QToF mass

558 spectrometer connected to a 1290 series chromatographic system with a Kinetex® 2.6 µ HILIC  
559 column (100 Å, 150 x 2.1 mm) in negative mode. The most abundant GPDGDAG was quantified  
560 with the following transition (MS1 m/z: 1071.6, MS2 m/z: 153.0). Integrated peak areas were  
561 normalized against cell weight.

562

### 563 **RNA Sequencing**

564 Sequencing of RNA was done from OG1RF,  $\Delta mprF1$ ,  $\Delta mprF2$ , and  $\Delta mprF1\Delta mprF2$  strains.  
565 Detailed methods are described in the supplementary information file. RNAseq files are available  
566 on NCBI, Sequence Read Archive (SRA) (Accession: PRJNA634972).

567

### 568 **Analysis of acyl-ACP content**

569 Quantification of acyl-ACPs were done as previously described with the following modifications  
570 (39, 40). 20 mL of overnight cultures were pelleted, treated with 10 mg/mL of lysozyme solution  
571 for 1 hour and lysed using a probe sonicator at 40% amplitude for 2 minutes (pulsed at 30s on  
572 and 30 s off) for 2 cycles. Unlysed cells were removed by centrifugation at 15 700 rcf for 30  
573 minutes at 4°C and the concentration of proteins within the clarified lysate was then measured  
574 using the Qubit Protein Assay (ThermoFisher Scientific, USA) according to the manufacturer's  
575 instructions. 50 µL of <sup>15</sup>N acyl-ACP standards (Holo, 2:0, 3:0, 4:0, 6:0, 8:0, 10:0, 12:0, 13:0, 14:0,  
576 16:0, 18:0, 18:1) were then spiked into the sample at 5 µM equimolar concentrations. Proteins  
577 were precipitated from standard spiked lysates via TCA-precipitation and resuspended in 50mM  
578 MOPS buffer, pH 7.5. Resuspended proteins were then treated with the ASP-N protease at 20:1  
579 ratio (protein:enzyme) at 37°C overnight. Reaction was then stopped by addition of methanol to a  
580 final concentration of 50%. These samples were then analysed using LC-MS with MRMs using  
581 previously described solvent gradients and MRM parameters (39). An Agilent 6495A QqQ mass  
582 spectrometer connected to a 1290 series chromatographic system was used with a Discovery  
583 BIO Wide pore C18-3 (10cm x 2.1mm, 3µM particle size) (Supelco, USA). Electrospray ionization  
584 (ESI) was used to ionize lipids. Acquisition was carried out with the following source parameters:  
585 gas temperature: 290°C, gas flow: 12 L/min, nebulizer: 30 psi, sheath gas heater: 400°C, sheath  
586 gas flow: 11 L/min, capillary: 4500 V, Vcharging: 1500 V. Signal intensities were normalized to  
587 the spiked internal standards to obtain relative measurements and further normalized against the  
588 initial protein concentration.

589

### 590 **Fatty acid methyl esters (FAME) analysis**

591 Late stationary phase cultures of wild type and  $\Delta mprF1\Delta mprF2$  grown in either BHI (overnight) or  
592 CDM (72 hours) were lyophilized and sent together with powdered BHI for GC-FAME analysis at  
593 the Identification Service of Deutsche Sammlung von Mikroorganismen und Zellkulturen GmbH  
594 (DSMZ), Braunschweig, Germany. Cellular fatty acids were converted into fatty acid methyl  
595 esters (FAME) and analyzed by GC-MS using used C<sub>21:0</sub> FAME in a defined amount per biomass  
596 as internal standard for normalization.

597

### 598 **Radiolabeling and thin layer chromatography (TLC)**

599 Radiolabeling of lipids were performed as previously described with the following modifications  
600 (56) [<sup>14</sup>C]-acetate or [<sup>32</sup>P]-disodium phosphate (Perkin Elmer, USA) was added into 5 mL of  
601 media at 0.2 µCi/mL or 1 µCi/mL respectively before culturing strains overnight at 37°C for 16-18  
602 hours at static conditions. Lipids were then extracted as previously described and resuspended in  
603 50 µL of chloroform-methanol solution (1:1 v/v) (10). 10 µL of lipid extracts were mixed with 2 mL  
604 of Ultima Gold™ scintillation fluid (Perkin Elmer, USA), and radioactive counts were measured  
605 using a MicroBeta2® scintillation counter (Perkin Elmer, USA). The lipid extracts were spotted on  
606 to silica-gel coated TLC plates (Merck, USA) and normalized according to the scintillation counts.  
607 TLC plates were developed in pre-equilibrated TLC chambers with chloroform:methanol:water  
608 (65:25:4) solvent system for 1-dimension (1D) TLCs. For 2-dimensional (2D) TLCs, TLC plates  
609 were developed using chloroform:methanol:water (65:25:4) solvent system for the first dimension  
610 and chloroform:hexane:methanol:acetic acid (50:30:10:5) for the second dimension. TLC plates  
611 were then visualized by exposure to a storage phosphor screen (GE healthcare, USA) overnight,

612 and read using a Storm Phosphorimager (GE healthcare, USA). For iodine and ninhydrin-stained  
613 TLC plates, no radiolabeling was carried out and TLC spots were normalized based on dry cell  
614 weight instead. Iodine crystals (Sigma-Aldrich, USA) were used to develop TLC plates in a  
615 chamber, while for ninhydrin staining, ninhydrin was applied to the plates, allowed to air dry  
616 before heating with a hairdryer till spots appeared.

617

#### 618 **SDS-PAGE and western blot**

619 SDS-PAGE and western blot were performed as described in a previous study (57). 4-12% or  
620 12% NuPAGE® Bis-Tris mini gel in a XCell SureLock® Mini-Cell filled with either 1x MES or 1x  
621 MOPs SDS running buffer (Invitrogen, USA) was used and run at 140 V for 90 min. Proteins were  
622 transferred to nitrocellulose membranes using the iBlot™ Dry Blotting System (Invitrogen, USA)  
623 according to the manufacturer's protocol. The antibodies and developing solutions used are  
624 shown in **Table S1E**.

625

#### 626 **Bulk secretion assay**

627 Late stationary phase cultures were prepared by growing cultures in BHI broth overnight for 16-18  
628 hours at 37°C, static conditions. OD<sub>600</sub> readings of the cultures were measured. Cell-free  
629 supernatants were obtained by centrifugation at 6,000 rcf for 5 minutes at 4°C and filtering the  
630 supernatants into fresh Eppendorf tubes using 0.2 µm syringe filters. 1.6 mL of filtered  
631 supernatant was mixed with 400 µL of 100% w/v trichloroacetic acid (TCA) solution (1:4 ratio of  
632 TCA to sample) and incubated at 4°C for 10 minutes. Tubes were centrifuged at 20,000 rcf for 15  
633 minutes at 4°C. The precipitated protein pellet was washed once with 2 mL of 100% ice-cold  
634 acetone and placed on a 98°C heat block to evaporate residual acetone. The pellets were  
635 resuspended in 500 µL of PBS. Twenty-five microliters of these protein solutions were used for  
636 estimation of protein content using the Pierce BCA Protein Assay Kit (ThermoFisher, USA) in a  
637 microtiter plate format according to the manufacturer's protocol. Protein concentrations of the  
638 samples were then normalized to OD<sub>600</sub> of 1.0 based on the respective OD<sub>600</sub> readings of the  
639 individual cultures.

640

#### 641 **Alkaline phosphatase (AP) secretion assay**

642 Secretion of the strains were monitored by its ability to secrete a chimeric alkaline phosphatase,  
643 PhoZF (*E. faecalis* native PhoZ fused to the secretion domain of protein F from *S. pyogenes*)  
644 PhoZF secretion monitored by its ability to convert para-nitrophenyl phosphate (pNPP) into a  
645 colored product that can be measured by absorbance at 405 nm. Mid-log phase cultures of  
646 strains harboring the pABG5 plasmid containing the chimeric alkaline  
647 phosphatase enzyme (PhoZF) were normalized to OD<sub>600</sub> of 0.5. Cell-free supernatants were  
648 obtained by centrifuging samples at 6,000 rcf for 5 minutes at 4°C and filtering the supernatant  
649 through 0.2 µm syringe filters. 25 µL of supernatant was added to 200 µL of 1M Tris-HCl, pH 8.0,  
650 in a 96-well microtitre plates. 25 µL of 4 mg/mL para-nitrophenyl phosphate (pNPP) (Sigma-  
651 Aldrich, USA) was then added to each well to start the reaction. The plate was then placed into a  
652 Tecan Infinite® M200 Pro spectrophotometer and incubated at 37°C with the absorbance read at  
653 405 nm every 10 minutes for 18 hours.

654

#### 655 **Analyzing membrane fluidity by Laurdan staining (microscopy)**

656 Late stationary and mid-log phase cultures were normalized to OD<sub>600</sub> of 0.7 in PBS and incubated  
657 with 100 µM of Laurdan for 10 minutes at 37°C. Cells were washed twice with PBS and 10 µL of  
658 the cell suspension was spotted onto PBS-agarose pads (1% w/v) mounted on glass slides.  
659 Coverslips were placed over the agarose pads and sealed using paraffin wax.

660

661 Slides were imaged using a Zeiss LSM 880 Laser Scanning Microscope with Airyscan, using a  
662 Plan-Apochromat 63x/1.4 Oil DIC objective with an incubation chamber set to 37°C. The slides  
663 were equilibrated for 10 minutes within the chamber before imaging and excited using a 405nm  
664 laser with emission collected between 419-455nm (blue) and 480-520nm (green) simultaneously.  
665 Digital images were acquired using the Zen (Zeiss) software and analyzed using ImageJ. Using

666 ImageJ, regions of interests (ROIs) of individual cells or cell clusters were selected and mean  
667 fluorescence intensities (MFIs) of each ROI for each channel were measured and tabulated in  
668 Microsoft excel. Using the following formula, the average GP values for each ROI were calculated  
669 and then plotted using Graphpad Prism software:  
670

$$671 \quad GP = \frac{I_{Blue} - I_{Green}}{I_{Blue} + I_{Green}} = \frac{I_{419-455 \text{ nm}} - I_{480-520 \text{ nm}}}{I_{419-455 \text{ nm}} + I_{480-520 \text{ nm}}}$$

672  
673 Laurdan was validated to be responsive to changes in membrane fluidity via control experiments  
674 subjecting stained cells to a gradient of temperatures, and membrane fluidizer, benzyl alcohol  
675 (**Fig. S7B, C**).

#### 677 **Daptomycin minimum inhibitory concentration (MIC)**

678 Mid-log phase cultures of the strains were tested for their daptomycin minimum inhibitory  
679 concentration (MIC) using the microplate broth dilution methods as previously described (10).

680

#### 681 **Static biofilm assay with crystal violet staining**

682 Static biofilm assays with crystal violet staining were performed as previously described on the  
683 wild type,  $\Delta mprF1$ ,  $\Delta mprF2$ , and  $\Delta mprF1 \Delta mprF2$  across a 5-day period (58).

684

#### 685 **Antimicrobial Peptide (AMP) Susceptibility Assays**

686 Overnight OG1RF cultures were subcultured in BHI liquid broth at a 1:10 dilution and grown to  
687 mid-log phase ( $OD_{600} 0.5 \pm 0.05$ ). These bacterial cultures were then normalized to  $OD_{600} 0.5$  and  
688 harvested by centrifugation at 6,000 rcf for 5 minutes at 4°C. The supernatant was discarded and  
689 the remaining cell pellet was washed and resuspended in 1 mL of 0.01 M low-salt phosphate  
690 buffer (PB). Bacterial resuspensions were then serially diluted 500-fold and 25  $\mu$ L of each sample  
691 was added twice into a 96-well microtiter plate, for a total of 2 technical replicates. An equal  
692 volume of human  $\beta$ -defensin 2 (hBD2) or LL-37 (Peptide Institute Inc., Japan) was added to the  
693 samples and incubated statically for 2 hours at 37°C (**Table S1G**). Serial dilution was then  
694 performed up to  $10^{-8}$  using 1X sterile phosphate buffered saline (PBS). 5  $\mu$ L of bacterial  
695 suspension from each well was then spotted 3 times onto a BHI agar plate, for a total of 6  
696 technical replicates per sample. The spotted agar plates were then incubated statically overnight  
697 at 37°C and surviving bacteria were determined by CFU enumeration.

698

#### 699 **Acknowledgments**

700

701 This work was supported by the National Research Foundation and Ministry of Education (MOE)  
702 Singapore under its Research Centre of Excellence Program, and by an MOE AcRF Tier 1 grant  
703 (MOE2017-T1-001-269) and a National Medical Research Council (NMRC) grant (OFIRG20nov-  
704 0079), both awarded to KAK. Work in the MRW laboratory was supported by grants from the  
705 National University of Singapore via the Life Sciences Institute (LSI), the National Research  
706 Foundation (NRFSPB-P4) and the NRF and A\*STAR IAF-ICP I1901E0040. SLC was supported  
707 by National Medical Research Council (NMRC) grants (NMRC/CIRG/1358/2013 and  
708 NMRC/OFIRG/0009/2016). SSC acknowledges support from the Singapore Ministry of Health  
709 National Medical Research Council under its Open Fund Individual Research Grant (MOH-  
710 000145). DKA and SAM acknowledge support from U.S. Department of Agriculture-Agricultural  
711 Research Service and the National Science Foundation Major Research Instrumentation  
712 program, award #DBI-1427621 that funded a mass spectrometer used in aspects of the project.  
713 We thank Adeline Mei Hui Yong for help with RNA extractions and Tan Wee Boon for assisting  
714 with the radiolabeling of lipids.

715

#### 716 **References**

717 1. Murray BE. 1990. The life and times of the Enterococcus. Clin Microbiol Rev 3:46-65.

- 718 2. Kristich C, Rice L, Arias C. 2014. Enterococcal Infection—Treatment and Antibiotic  
719 Resistance. *In* Gilmore M, Clewell D, Ike Y, Shankar N (ed), *Enterococci: From*  
720 *Commensals to Leading Causes of Drug Resistant Infection*. Massachusetts Eye and Ear  
721 Infirmary, Boston. <https://www.ncbi.nlm.nih.gov/books/NBK190424/>.
- 722 3. Ch'ng JH, Chong KKL, Lam LN, Wong JJ, Kline KA. 2019. Biofilm-associated infection by  
723 enterococci. *Nat Rev Microbiol* 17:82-94.
- 724 4. Zasloff M. 2002. Antimicrobial peptides of multicellular organisms. *Nature* 415:389-395.
- 725 5. Peschel A, Sahl H. 2006. The co-evolution of host cationic antimicrobial peptides and  
726 microbial resistance. *Nat Rev Micro* 4:529-536.
- 727 6. Durr U, Sudheendra U, Ramamoorthy A. 2006. LL-37, the only human member of the  
728 cathelicidin family of antimicrobial peptides. *Biochim Biophys Acta* 1758.
- 729 7. Ganz T. 2001. Defensins: antimicrobial peptides of innate immunity. *Nat Rev Immunol*  
730 3:710-720.
- 731 8. Rashid R, Veleba M, Kline K. 2016. Focal Targeting of the Bacterial Envelope by  
732 Antimicrobial Peptides. *Front Cell Dev Biol* 4:55.
- 733 9. Kandaswamy K, Liew T, Wang C, Huston-Warren E, Meyer-Hoffert U, Hultenby K,  
734 Schröder J, Caparon M, Normark S, Henriques-Normark B, Hultgren S, Kline K. 2013.  
735 Focal targeting by human  $\beta$ -defensin 2 disrupts localized virulence factor assembly sites  
736 in *Enterococcus faecalis*. *Proc Natl Acad Sci U S A* 110:20230-35.
- 737 10. Rashid R, Cazenave-Gassiot A, Gao I, Nair Z, Kumar J, Gao L, Kline K, Wenk M. 2017.  
738 Comprehensive analysis of phospholipids and glycolipids in the opportunistic pathogen  
739 *Enterococcus faecalis*. *PLOS One* 12:e0175886.
- 740 11. dos Santos Mota J, den Kamp J, Verheij H, van Deenen L. 1970. Phospholipids of  
741 *Streptococcus faecalis*. *J Bacteriol* 104:611-9.
- 742 12. Peschel A, Jack R, Otto M, Collins L, Staubitz P, Nicholson G, Kalbacher H,  
743 Nieuwenhuizen W, Jung G, Tarkowski A, van Kessel K, van Strijp J. 2001. *Staphylococcus*  
744 *aureus* resistance to human defensins and evasion of neutrophil killing via the novel  
745 virulence factor MprF is based on modification of membrane lipids with l-lysine. *J Exp*  
746 *Med* 193:1067-76.
- 747 13. Samant S, Hsu F, Neyfakh A, Lee H. 2009. The *Bacillus anthracis* protein MprF is required  
748 for synthesis of lysylphosphatidylglycerols and for resistance to cationic antimicrobial  
749 peptides. *J Bacteriol* 191:1311-9.
- 750 14. Bao Y, Sakinc T, Laverde D, Wobser D, Benachour A, Theilacker C, Hartke A, Huebner J.  
751 2012. Role of mprF1 and mprF2 in the pathogenicity of *Enterococcus faecalis*. *PLoS One*  
752 7.
- 753 15. Ernst C, Kuhn S, Slavetinsky C, Krismer B, Heilbronner S, Gekeler C, Kraus D, Wagner S,  
754 Peschel A. 2015. The lipid-modifying multiple peptide resistance factor is an oligomer  
755 consisting of distinct interacting synthase and flippase subunits. *mBio* 6:e02340-14.
- 756 16. Ernst CM, Staubitz P, Mishra NN, Yang S-J, Hornig G, Kalbacher H, Bayer AS, Kraus D,  
757 Peschel A. 2009. The bacterial defensin resistance protein MprF consists of separable  
758 domains for lipid lysinylation and antimicrobial peptide repulsion. *PLoS Pathog*  
759 5:e1000660.
- 760 17. Thedieck K, Hain T, Mohamed W, Tindall BJ, Nimtz M, Chakraborty T, Wehland J, Jänsch  
761 L. 2006. The MprF protein is required for lysinylation of phospholipids in listerial  
762 membranes and confers resistance to cationic antimicrobial peptides (CAMPs) on  
763 *Listeria monocytogenes*. *Molecular Microbiology* 62:1325-1339.

- 764 18. Ernst C, Peschel A. 2011. Broad-spectrum antimicrobial peptide resistance by MprF-  
765 mediated aminoacylation and flipping of phospholipids. *Mol Microbiol* 80:290-9.
- 766 19. Woodall B, Harp J, Brewer W, Tague E, Campagna S, Fozo E. 2021. *Enterococcus faecalis*  
767 Readily Adapts Membrane Phospholipid Composition to Environmental and Genetic  
768 Perturbation. *Front Microbiol* 12.
- 769 20. Mishra N, Bayer A, Tran T, Shamoo Y, Mileykovskaya E, Dowhan W, Guan Z, Arias C.  
770 2012. Daptomycin resistance in enterococci is associated with distinct alterations of cell  
771 membrane phospholipid content. *PLoS One* 7.
- 772 21. Tran T, Panesso D, Mishra N, Mileykovskaya E, Guan Z, Munita J, Reyes J, Diaz L,  
773 Weinstock G, Murray B, Shamoo Y, Dowhan W, Bayer A, Arias C. 2013. Daptomycin-  
774 resistant *Enterococcus faecalis* diverts the antibiotic molecule from the division septum  
775 and remodels cell membrane phospholipids. *mBio* 4:e00281-13.
- 776 22. Chwastek G, Surma M, Rizk S, Grosser D, Lavrynenko O, Rucińska M, Jambor H, Sáenz J.  
777 2020. Principles of Membrane Adaptation Revealed through Environmentally Induced  
778 Bacterial Lipidome Remodeling. *Cell Rep* 32:108165.
- 779 23. Bleffert F, Granzin J, Caliskan M, Schott-Verdugo S, Siebers M, Thiele B, Rahme L,  
780 Felgner S, Dörmann P, Gohlke H, Batra-Safferling R, Jaeger K, Kovacic F. 2022. Structural,  
781 mechanistic, and physiological insights into phospholipase A-mediated membrane  
782 phospholipid degradation in *Pseudomonas aeruginosa*. *eLife* 11.
- 783 24. Rashid R, Cazenave-Gassiot A, Gao I, Nair Z, Kumar J, Liang G, Kline K, Wenk M. 2017.  
784 Comprehensive Analysis of Phospholipids and Glycolipids in the Opportunistic Pathogen  
785 *Enterococcus faecalis* *PLOS One* 12:e0175886.
- 786 25. Luo H, Lin Y, Gao F, Zhang C, Zhang R. 2014. DEG 10, an update of the database of  
787 essential genes that includes both protein-coding genes and noncoding genomic  
788 elements. *Nucleic Acids Res* 42:D574–D580.
- 789 26. Hebecker S, Krausze J, Hasenkampf T, Schneider J, Groenewold M, Reichelt J, Jahn D,  
790 Heinz D, Moser J. 2015. Structures of two bacterial resistance factors mediating tRNA-  
791 dependent aminoacylation of phosphatidylglycerol with lysine or alanine. *Proc Natl Acad*  
792 *Sci U S A* 112:10691-6.
- 793 27. Heacock PN, Dowhan W. 1987. Construction of a lethal mutation in the synthesis of the  
794 major acidic phospholipids of *Escherichia coli*. *J Biol Chem* 262:13044-9.
- 795 28. Dowhan W. 1997. Molecular basis for membrane phospholipid diversity: Why Are There  
796 So Many Lipids? *Annual Review of Biochemistry* 66:199-232.
- 797 29. Furse S. 2016. Is phosphatidylglycerol essential for terrestrial life? *Journal of chemical*  
798 *biology* 10:1-9.
- 799 30. Percy M, Gründling A. 2014. Lipoteichoic acid synthesis and function in gram-positive  
800 bacteria. *Annu Rev Microbiol* 68:81-100.
- 801 31. Rahman O, Dover L, Sutcliffe I. 2009. Lipoteichoic acid biosynthesis: two steps forwards,  
802 one step sideways? *Trends Microbiol* 17:219-225.
- 803 32. Saito HE, Harp JR, Fozo EM. 2017. *Enterococcus faecalis* Responds to Individual  
804 Exogenous Fatty Acids Independently of Their Degree of Saturation or Chain Length.  
805 *Applied and environmental microbiology* 84:e01633-17.
- 806 33. Eckhardt T, Skotnicka D, Kok J, Kuipers O. 2013. Transcriptional regulation of fatty acid  
807 biosynthesis in *Lactococcus lactis*. *Journal of Bacteriology* 195:1081-1089.
- 808 34. Lu Y, Rock C. 2006. Transcriptional regulation of fatty acid biosynthesis in *Streptococcus*  
809 *pneumoniae*. *Mol Microbiol* 59:551-66.

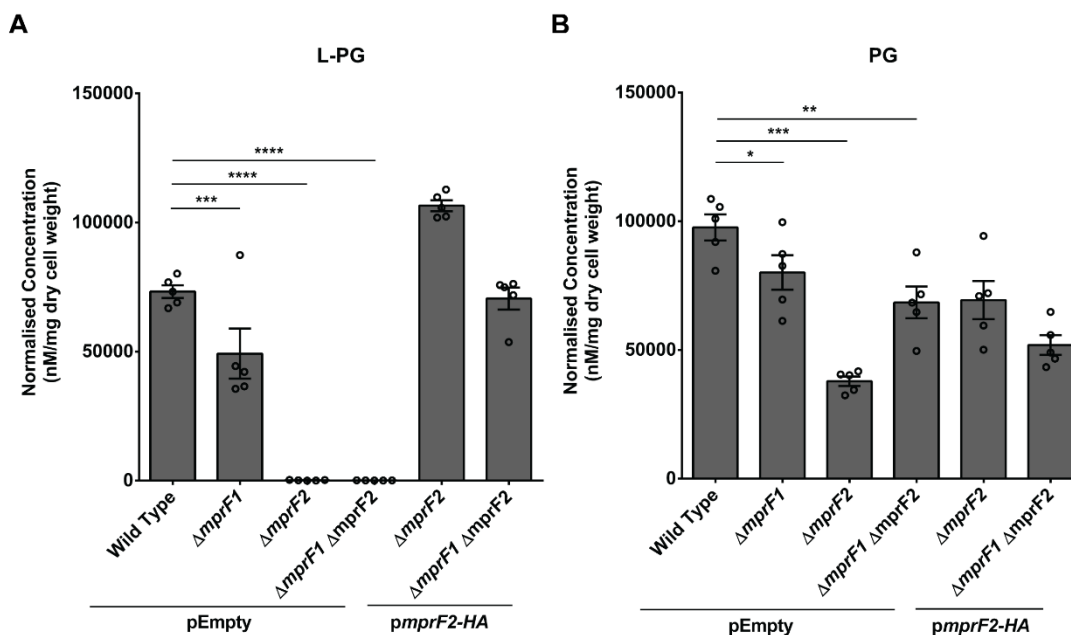


- 810 35. Jerga A, Rock C. 2009. Acyl-Acyl carrier protein regulates transcription of fatty acid  
811 biosynthetic genes via the FabT repressor in *Streptococcus pneumoniae*. *The Journal of*  
812 *Biological Chemistry* 284:15364-15368.
- 813 36. Cronan J. 2014. The chain-flipping mechanism of ACP (acyl carrier protein)-dependent  
814 enzymes appears universal. *Biochem J* 460:157-63.
- 815 37. Yao J, Rock C. 2017. Exogenous fatty acid metabolism in bacteria. *Biochimie* 141:30-39.
- 816 38. Zhu L, Zou Q, Cao X, Cronan J. 2019. *Enterococcus faecalis* Encodes an Atypical Auxiliary  
817 Acyl Carrier Protein Required for Efficient Regulation of Fatty Acid Synthesis by  
818 Exogenous Fatty Acids. *mBio* 10:e00577-19.
- 819 39. Nam J, Jenkins L, Li J, Evans B, Jaworski J, Allen D. 2020. A General Method for  
820 Quantification and Discovery of Acyl Groups Attached to Acyl Carrier Proteins in Fatty  
821 Acid Metabolism Using LC-MS/MS. *Plant Cell* 32:820-832.
- 822 40. Jenkins L, Nam J, Evans B, Allen D. 2021. Quantification of Acyl-Acyl Carrier Proteins for  
823 Fatty Acid Synthesis Using LC-MS/MS. *Methods Mol Biol* 2295:219-247.
- 824 41. de Vrije T, de Swart R, Dowhan W, Tommassen J, de Kruijff B. 1988. Phosphatidylglycerol  
825 is involved in protein translocation across *Escherichia coli* inner membranes. *Nature*  
826 334:173-5.
- 827 42. van Dalen A, de Kruijff B. 2004. The role of lipids in membrane insertion and  
828 translocation of bacterial proteins. *Biochim Biophys Acta* 1694:97-109.
- 829 43. Alberts BJ, A.; Lewis, J.; Raff, M.; Roberts, K. ; Walter, P. 2002. *Molecular biology of the*  
830 *cell*. 4th edition., *The Lipid Bilayer*, 4th ed. Garland Science, New York.
- 831 44. Bach J, Bramkamp M. 2013. Flotillins functionally organize the bacterial membrane. *Mol*  
832 *Microbiol* 88:1205-17.
- 833 45. Harris FM, Best KB, Bell JD. 2002. Use of laurdan fluorescence intensity and polarization  
834 to distinguish between changes in membrane fluidity and phospholipid order. *Biochim*  
835 *Biophys Acta* 1565:123-8.
- 836 46. Luo Y, Javed M, Deneer H. 2018. Comparative study on nutrient depletion-induced  
837 lipidome adaptations in *Staphylococcus haemolyticus* and *Staphylococcus epidermidis*.  
838 *Scientific Reports* 8:2356.
- 839 47. Koch H, Haas R, Fischer W. 1984. The role of lipoteichoic acid biosynthesis in membrane  
840 lipid metabolism of growing *Staphylococcus aureus*. *Eur J Biochem* 138:357-363.
- 841 48. Hines K, Waalkes A, Penewit K, Holmes E, Salipante S, Werth B, Xu L. 2017.  
842 Characterization of the Mechanisms of Daptomycin Resistance among Gram-Positive  
843 Bacterial Pathogens by Multidimensional Lipidomics. *mSphere* 2:e00492-17.
- 844 49. Zou Q, Dong H, Zhu L, Cronan J. 2022. The *Enterococcus faecalis* FabT Transcription  
845 Factor Regulates Fatty Acid Biosynthesis in Response to Exogeneous Fatty Acids. *Front*  
846 *Microbiol* 13:877582.
- 847 50. Campo N, Tjalsma H, Buist G, Stepniak D, Meijer M, Veenhuis M, Westermann M, Müller  
848 J, Bron S, Kok J, Kuipers O, Jongbloed J. 2004. Subcellular sites for bacterial protein  
849 export. *Mol Microbiol* 53:1583-99.
- 850 51. Gold V, Robson A, Bao H, Romantsov T, Duong F, Collinson I. 2010. The action of  
851 cardiolipin on the bacterial translocon. *Proc Natl Acad Sci U S A* 107:10044-9.
- 852 52. Zemansky J, Kline B, Woodward J, Leber J, Marquis H, Portnoy D. 2009. Development of  
853 a mariner-based transposon and identification of *Listeria monocytogenes* determinants,  
854 including the peptidyl-prolyl isomerase PrsA2, that contribute to its hemolytic  
855 phenotype. *J Bacteriol* 191:3950-64.

- 856 53. Zhang Y, Rock C. 2008. Membrane lipid homeostasis in bacteria. *Nature Reviews*  
857 *Microbiology* 6:222-33.
- 858 54. Steinkühler J, Sezgin E, Urbančič I, Eggeling C, Dimova R. 2019. Mechanical properties of  
859 plasma membrane vesicles correlate with lipid order, viscosity and cell density. *Commun*  
860 *Biol* 2:337.
- 861 55. Ernst R, Ejsing C, Antonny B. 2016. Homeoviscous Adaptation and the Regulation of  
862 Membrane Lipids. *J Mol Biol* 428:4776-4791.
- 863 56. Shrivastava R, Jiang X, Chng S. 2017. Outer membrane lipid homeostasis via retrograde  
864 phospholipid transport in *Escherichia coli*. *Mol Microbiol* 106:395-408.
- 865 57. Nielsen HV, Guiton PS, Kline KA, Port GC, Pinkner JS, Neiers F, Normark S, Henriques-  
866 Normark B, Caparon MG, Hultgren SJ. 2012. The Metal Ion-Dependent Adhesion Site  
867 Motif of the *Enterococcus faecalis* EbpA Pilin Mediates Pilus Function in Catheter-  
868 Associated Urinary Tract Infection. *mBio* 3.
- 869 58. Lam L, Wong J, Chong K, Kline K. 2020. *Enterococcus faecalis* Manganese Exporter MntE  
870 Alleviates Manganese Toxicity and Is Required for Mouse Gastrointestinal Colonization.  
871 *Infect Immun* 88:e00058-20.

872

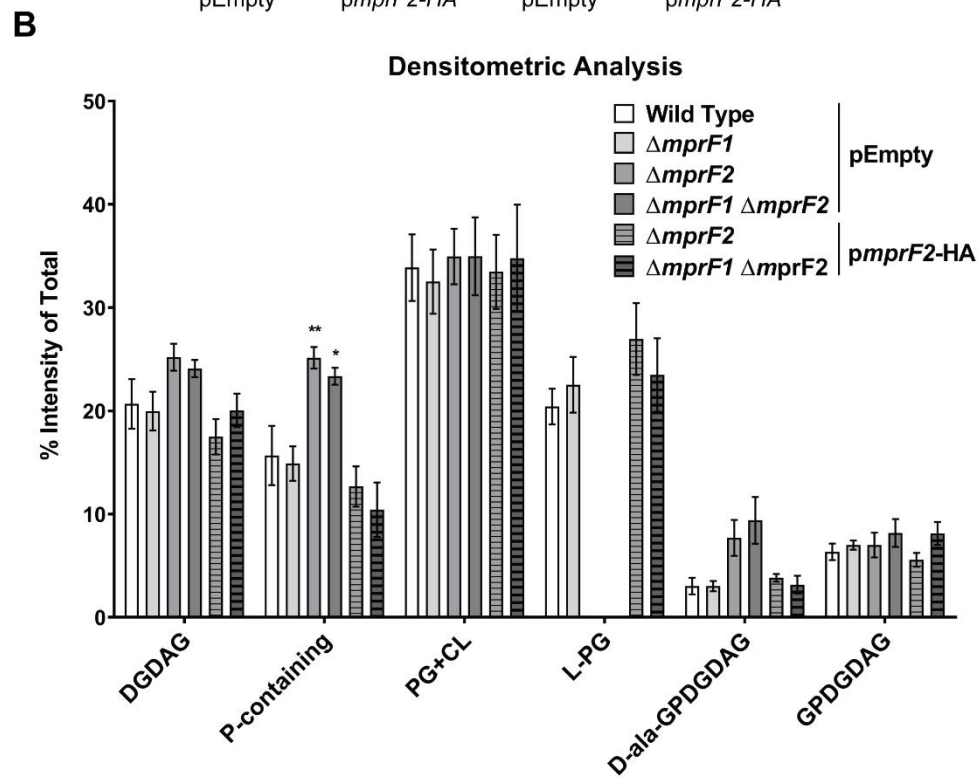
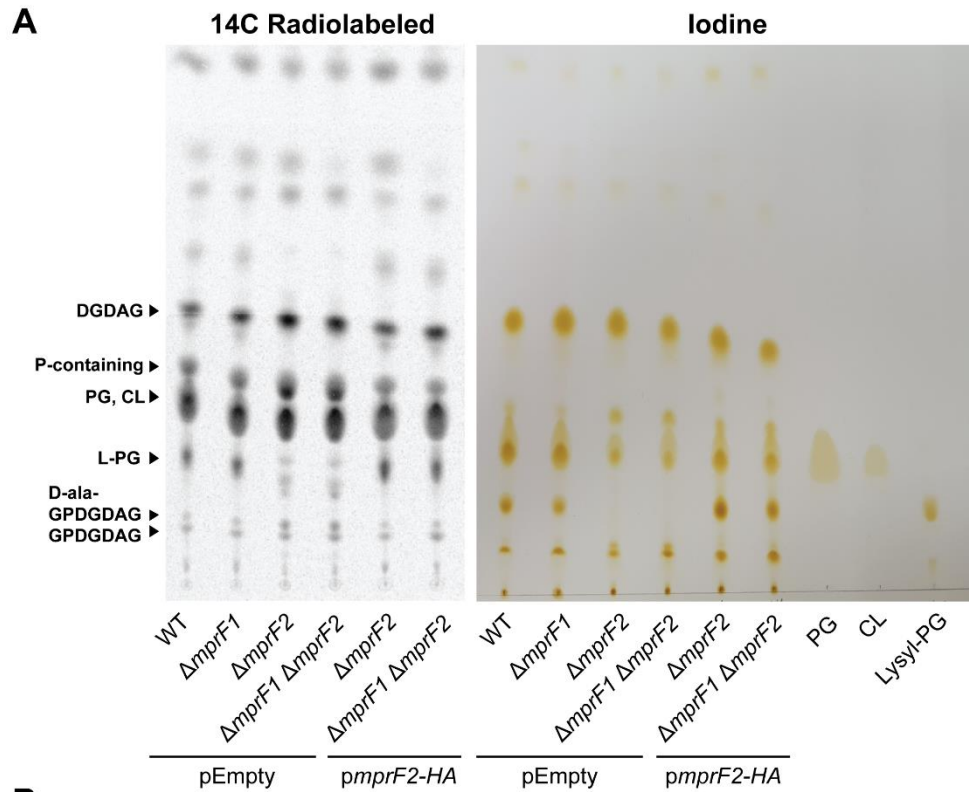
873 **Figures & Tables**

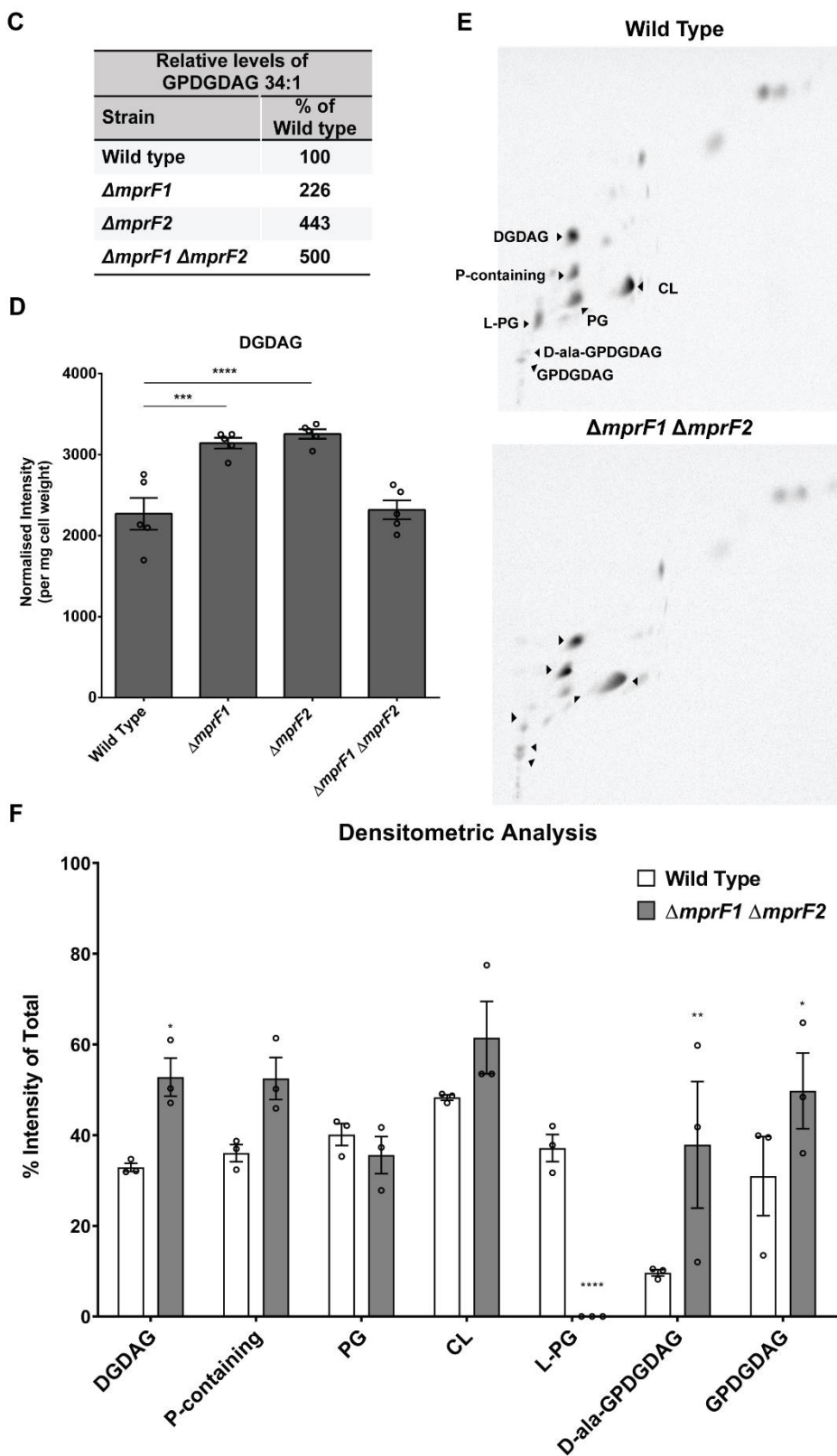


874

875 **Figure 1. *mprF* contributes to L-PG and PG levels.** Normalized amounts of total lysyl-  
876 phosphatidylglycerol (L-PG) **(A)** and total phosphatidylglycerol (PG) quantities **(B)** in *E. faecalis*  
877 wild type and *mprF* mutants are shown. These amounts were obtained by normalizing against  
878 internal standards and dry cell weight of the respective samples. *mprF2*-HA refers to *mprF2* with a  
879 hemagglutinin (HA) affinity tag on its C-terminal for ease of assessing expression. Data showing  
880 complementation with untagged *mprF2* can be found in **Fig. S1E-H**. Each bar represents the mean  
881  $\pm$  standard error of measurement calculated from 5 biological replicates, represented by each open  
882 circle. \*,  $p < 0.05$ ; \*\*,  $p < 0.01$ ; \*\*\*,  $p < 0.001$ ; \*\*\*\*,  $p < 0.0001$ ; Fisher's LSD test for ANOVA.

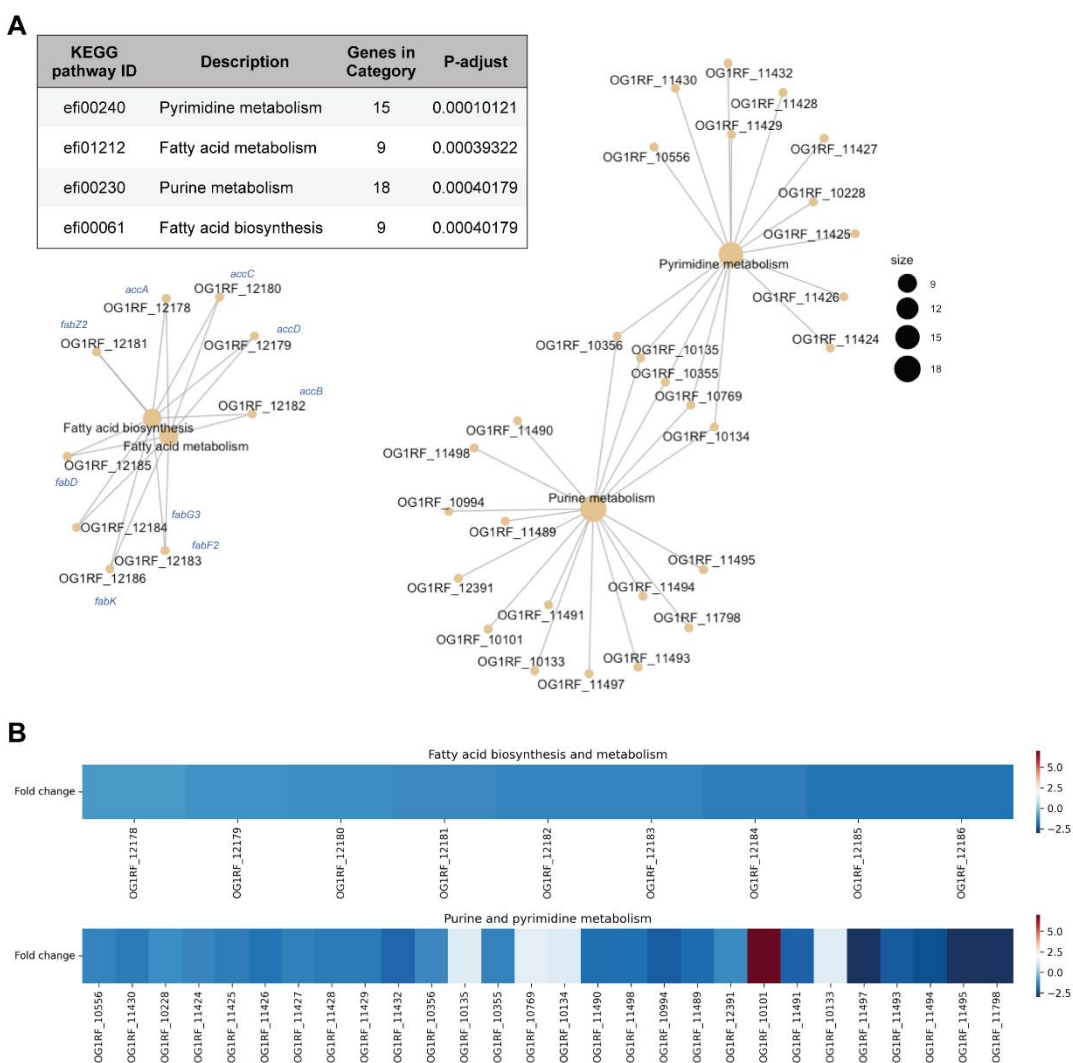
883





886 **Figure 2. *mprF* deletion results in changes in other lipid classes. (A)** Representative <sup>14</sup>C  
887 radiolabeled and iodine stained 1D-TLC of lipid extracts from the *mprF* mutants using chloroform:  
888 methanol: water (65:25:4). Standards were applied to the iodine-stained TLC plate to confirm the  
889 positions of PG, CL, and L-PG spots. Further identification of the other lipid spots can be found in  
890 the supplement (Supplementary Section 1 - TLC spot identification). **(B)** Densitometric analysis of  
891 <sup>14</sup>C radiolabeled 1D TLC spots. Each bar represents the mean ± standard error of measurement  
892 calculated from 4 biological replicates. **(C)** Semiquantitative analysis of dominant GPDGDAG  
893 species, GPDGDAG 34:1. **(D)** Semiquantitative quantification of DGDAG amounts across the  
894 *mprF* mutants. These amounts were obtained by normalizing against an external surrogate  
895 standard (MGDAG 34:1) and dry cell weights of the respective samples. Each bar represents the  
896 mean ± standard error of measurement calculated from 5 biological replicates. **(E)** Representative  
897 2D-TLC of lipid extracts from wild type and  $\Delta mprF1 \Delta mprF2$  for further spot separation to  
898 visualize changes in PG and CL. **(F)** Densitometric analysis of <sup>14</sup>C radiolabeled 2D TLC spots.  
899 Each bar represents the mean ± standard error of measurement calculated from 3 biological  
900 replicates. Statistical comparisons made for mutants against wild type. \*, p<0.05; \*\*, p<0.01; \*\*\*,  
901 p<0.001; \*\*\*\*, p<0.0001; Fisher's LSD test for ANOVA. Identities of these spots were determined  
902 through a combination of TLCs with lipid standards as well as mass spectrometry of the spots.  
903 Detailed information on how spot identities were assigned can be found in the supplement  
904 **(Supplementary Text 1A, Fig. S4, and Excel Table S1C).**

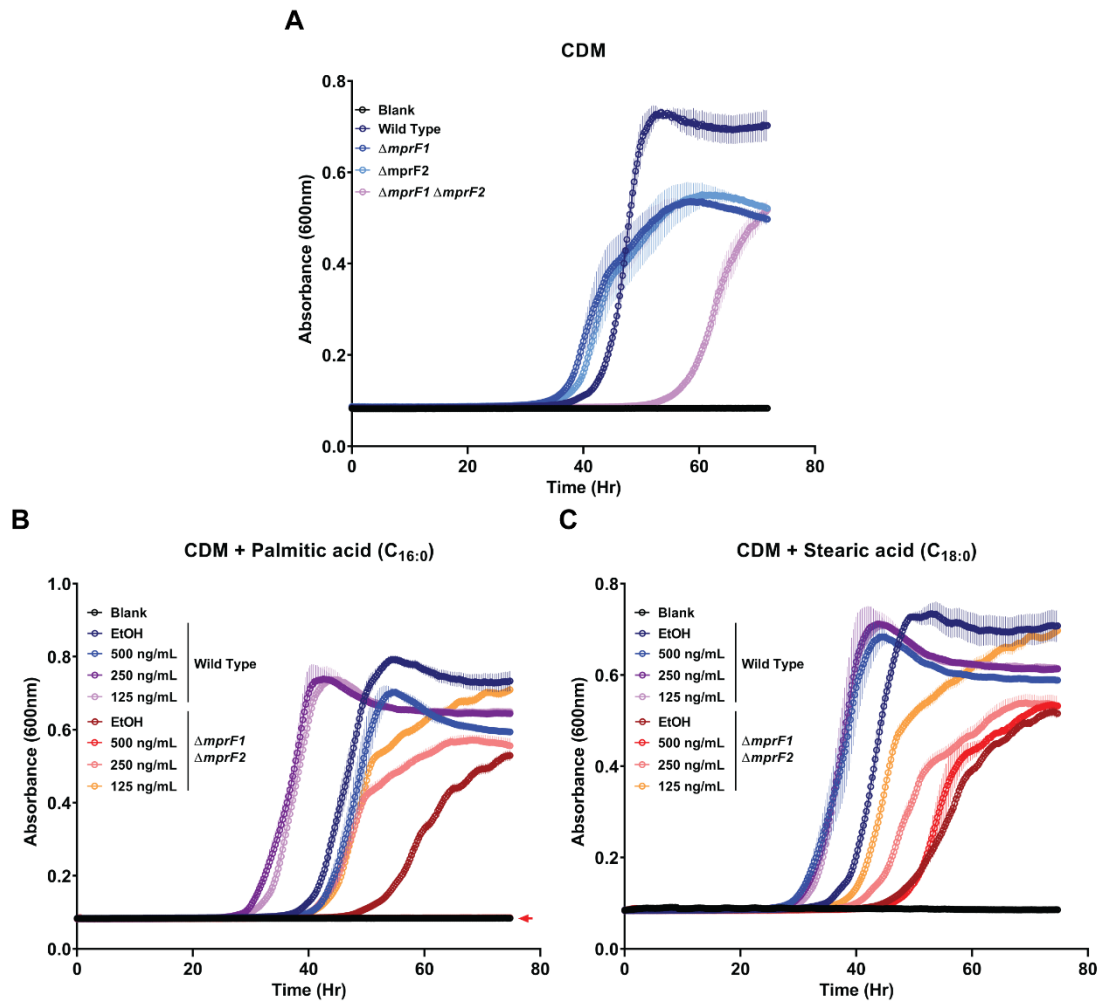
905



906

907 **Figure 3. Loss of *mprF* leads to changes in regulation of fatty acid biosynthesis and**  
 908 **nucleotide metabolism genes. (A)** Gene set enrichment analysis comparing KEGG categories of  
 909 differentially expressed genes between the parental wild type and  $\Delta mprF1 \Delta mprF2$ . The table  
 910 shows categories that are differentially regulated and the plots showing interconnectivity between  
 911 genes in each differentially regulated pathway. Node size corresponds to the number of enriched  
 912 genes. **(B)** Heatmap showing differential gene expression based on the gene set enrichment  
 913 analysis in **(A)**.

914

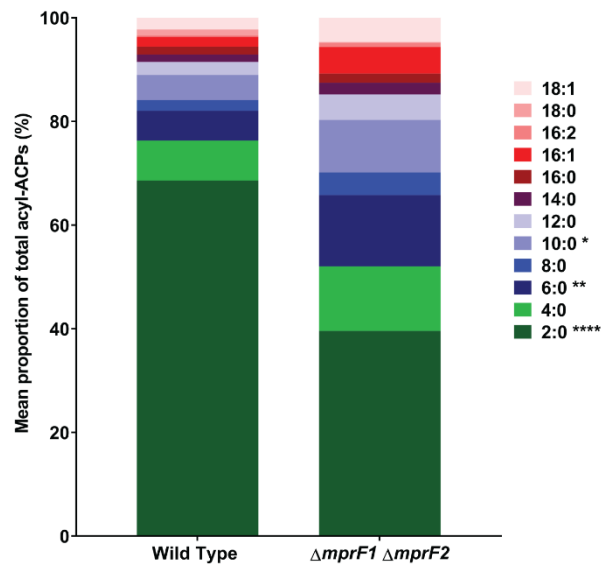


915

916 **Figure 4. *mprF* mutants possess a growth defect when grown in chemically defined media**  
917 **(CDM) which can be rescued by palmitic or stearic acid. (A)** Growth curves of wild type and  
918 *mprF* mutants grown in chemically defined media. Growth curves of wild type and  $\Delta mprF1$   
919  $\Delta mprF2$  grown under fatty acid supplementation of (B) palmitic acid (C<sub>16:0</sub>) or (C) stearic acid  
920 (C<sub>18:0</sub>). Equal volumes of ethanol (EtOH) were used as the solvent control for comparison. Each  
921 data point represents the mean  $\pm$  standard error of measurement calculated from 3 biological  
922 replicates averaged from 3 technical replicates each.  $\Delta mprF1 \Delta mprF2$  with 500 ng/mL palmitic  
923 acid in (B) is overlaid over the blank values as denoted by the colored arrow.

924



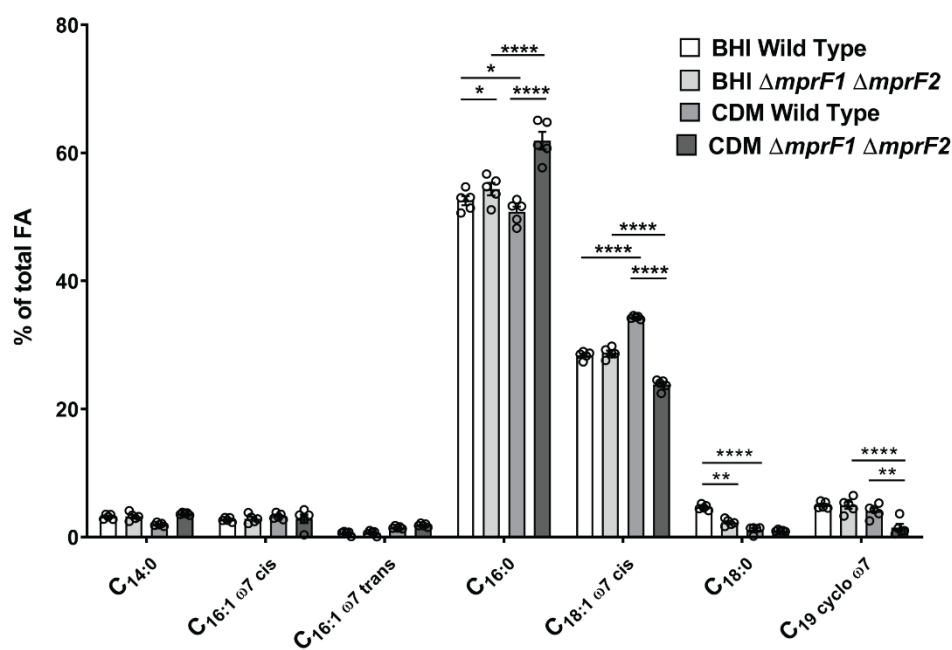


925

926 **Figure 5. *mprF* mutants display decreased proportions of short-chain acyl-acyl carrier**  
927 **proteins (acyl-ACPs).** Mean proportion of acyl-ACPs within WT and  $\Delta mprF1 \Delta mprF1$  derived  
928 from normalized concentrations measured using mass spectrometry. Data from 4 biological  
929 replicates was analyzed. Values were obtained by normalizing against a  $^{15}N$  acyl-ACP internal  
930 standard and total of protein concentration of the respective samples. Statistical comparisons  
931 made for  $\Delta mprF1 \Delta mprF2$  against wild type. \*,  $p < 0.05$ ; \*\*,  $p < 0.001$ ; \*\*\*\*,  $p < 0.0001$ ; Fisher's LSD  
932 test for ANOVA. Refer to **Fig. S7A** for values of each individual species.

933

934



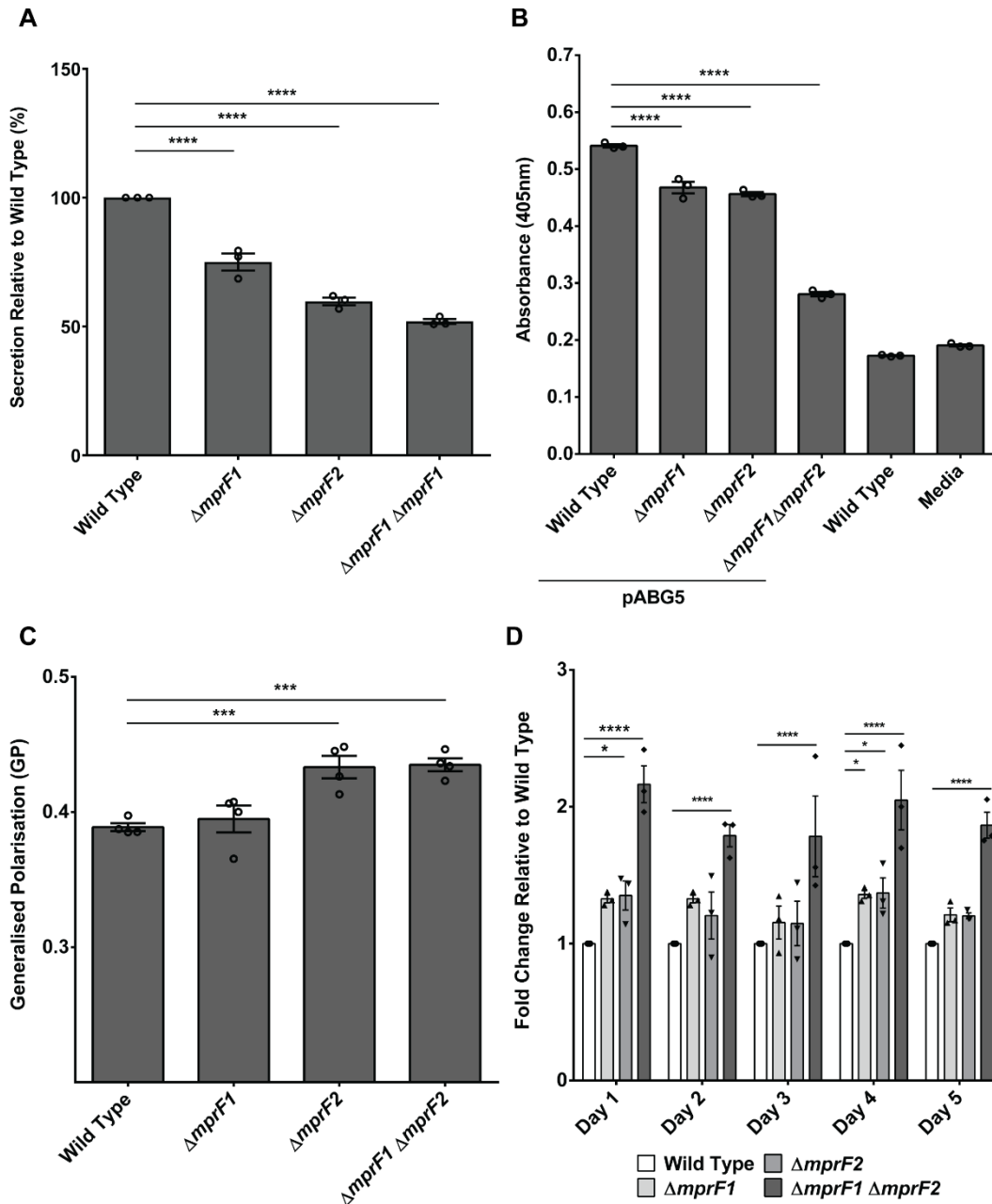
935

936 **Figure 6. *mprF* mutants possess an altered fatty acid profile when grown in CDM as**  
937 **compared to the wild type.** GC-FAME analysis of fatty acids in WT and  $\Delta mprF1 \Delta mprF2$  grown  
938 in either BHI or CDM. The most abundant fatty acid species that account for at least 1% or more  
939 of the total fatty acids (FA) present within the sample are displayed here. The full list of detected  
940 fatty acid methyl esters is shown in Excel **Table S1E**. Each bar represents the mean  $\pm$  standard  
941 error of measurement calculated from 5 biological replicates. \*, p<0.05; \*\*, p<0.01; \*\*\*\*,  
942 p<0.0001; Tukey test for ANOVA.

943

944

945

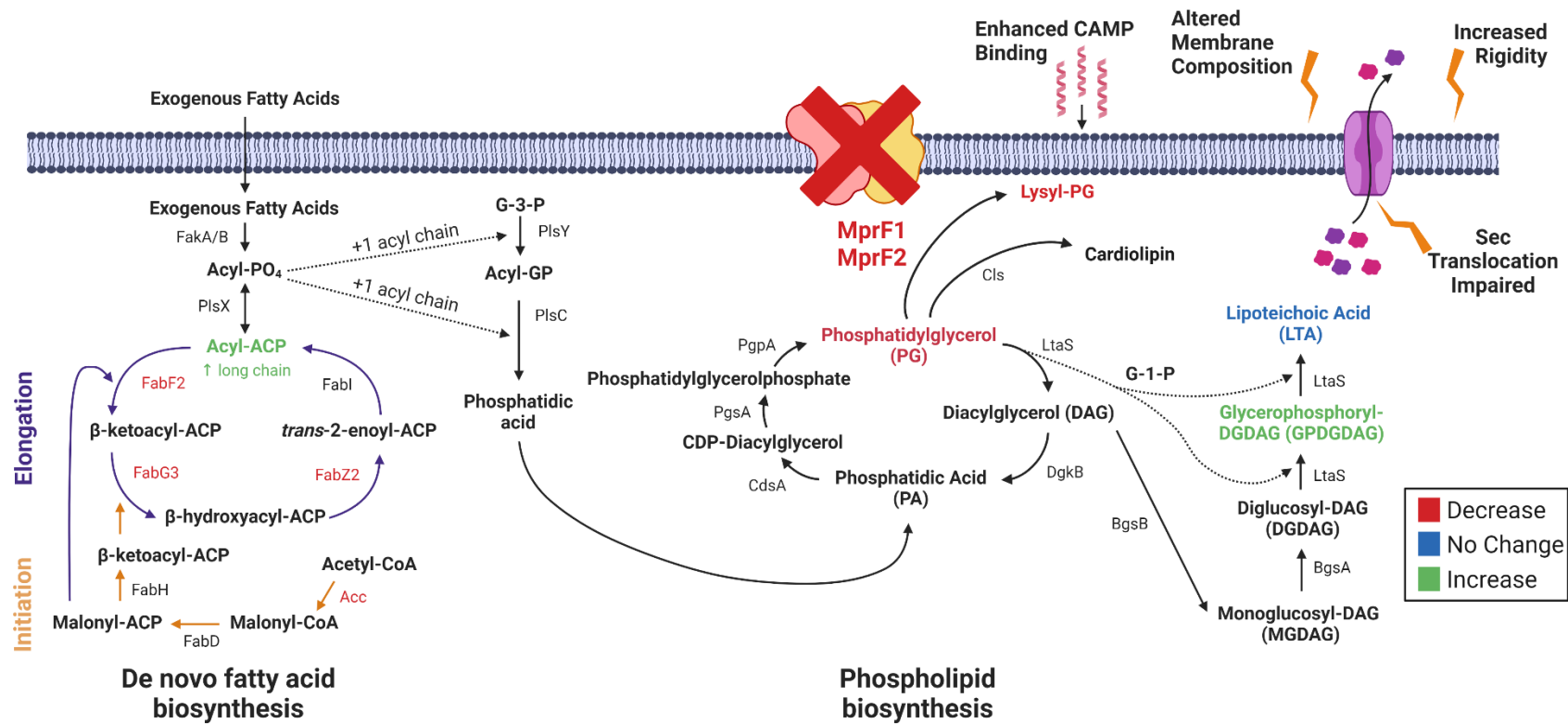


946

947 **Figure 7. *mprF* mutants exhibit pleiotropic phenotypes. (A)** Relative amounts of proteins  
 948 secreted into the growth media by wild type and mutant strains are shown. Each bar represents  
 949 the mean  $\pm$  standard error of the mean calculated from 3 biological replicates averaged from 3  
 950 technical replicates each. **(B)** Relative amounts of alkaline phosphatase (PhoZ encoded on the  
 951 plasmid pABG5, *E. faecalis* native PhoZ fused to the secretion domain of protein F from *S.*  
 952 *pyogenes*) secreted into the growth media by wild type and mutant strains growth to mid-  
 953 logarithmic phase are shown. PhoZ secretion was monitored by its ability to convert para-  
 954 nitrophenyl phosphate (pNPP) into a colored product that can be measured by absorbance at 405  
 955 nm. Each bar represents the mean  $\pm$  standard error of the mean calculated from 3 biological

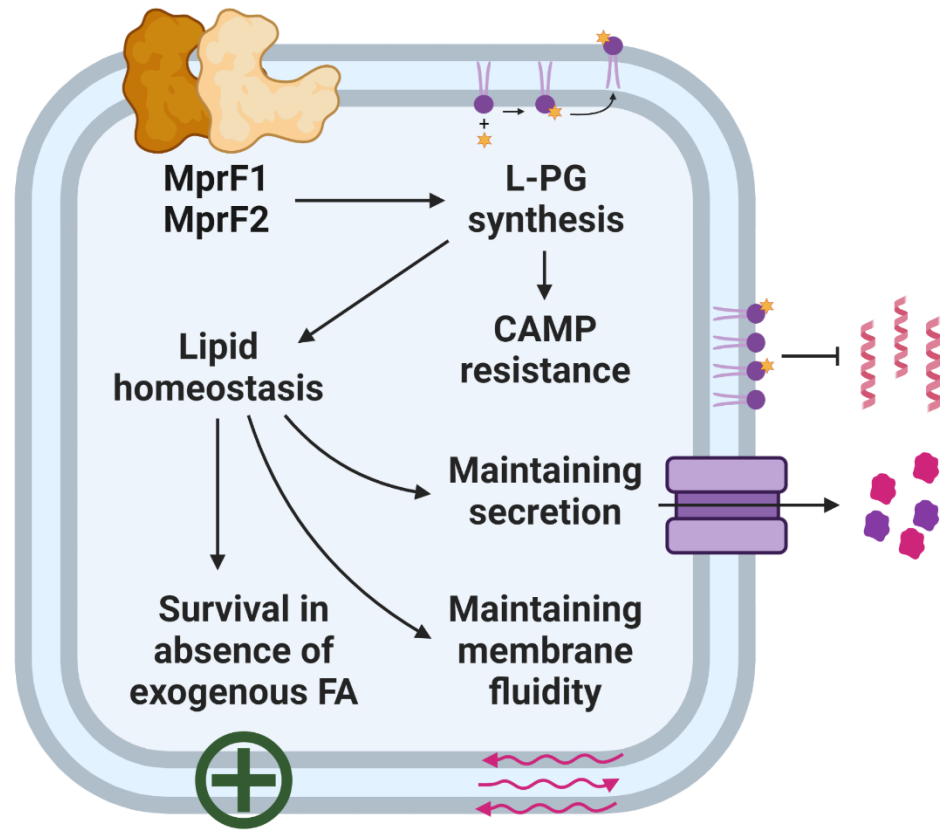
27

956 replicates averaged from 3 technical replicates each. **(C)** Cells were labeled with Laurdan and  
957 analyzed microscopically to assess for membrane fluidity changes. Higher GP values indicate  
958 more rigid membranes. Error bars represent the standard error of the mean of GP values from 4  
959 separate experiments. Each experiment consists of 1 biological replicate with average GP values  
960 tabulated from >100 ROIs of cells/cell clusters. (Controls to ensure that the Laurdan assay can  
961 sensitively and accurately measure differences in membrane fluidity can be found in **Fig. S7B,**  
962 **C**). **(D)** Static biofilm assay with crystal violet staining across 5-days. Relative fold-change of  
963 absorbance 595 nm readings of the crystal violet stain are reported with respect to the wild type.  
964 Each bar represents the mean  $\pm$  standard error of the mean calculated from 3 biological  
965 replicates averaged from 3 technical replicates each. \*,  $p<0.05$ ; \*\*\*,  $p<0.001$ ; \*\*\*\*,  $p<0.0001$ . All  
966 data sets were analyzed using Fisher's LSD test for ANOVA.



967

968 **Figure 8. A working model for lipidomic, transcriptomic, and phenotypic consequences following *mprF* deletion.** The loss of *mprF* leads to  
 969 downregulation of fatty acid biosynthesis genes and decreases in lysyl-PG (L-PG) and PG coupled with increases in GPDGDAG and a phosphorus-  
 970 containing lipid of unknown identity. These large lipidomic changes lead to functional impairment in Sec-mediated secretion, increased membrane  
 971 rigidity, and enhanced CAMP binding. Created with BioRender.com.  
 972



973

974

Graphical Abstract